Characteristic Mode Analysis of ESPAR for Single-RF MIMO Systems

Zixiang Han, *Graduate Student Member, IEEE*, Yujie Zhang, *Graduate Student Member, IEEE*, Shanpu Shen, *Member, IEEE*, Yue Li, *Student Member, IEEE*, Chi-Yuk Chiu, *Senior Member, IEEE*, and Ross Murch, *Fellow, IEEE*

***Abstract*— A systematic method based on the Theory of Characteristic Modes (TCM) for finding orthogonal radiation patterns of any electronically steerable parasitic array radiator (ESPAR) is described. This method can be useful for designing single-RF front-end multiple-input multiple-output (MIMO) systems in which orthogonal patterns can be utilized as a basis set for space modulation (SM) or full multiplexed MIMO systems. The method is based on the N-port formulation of TCM and is not restricted to antenna type or array configuration. It can also provide closed formed solutions for the antenna element currents required to generate the orthogonal patterns. In addition an approach to finding the required load reactances in ESPAR for generating the orthogonal patterns is provided and is based on the quasi-Newton method utilizing a closed form expression for the initial approximate solution. Approximate estimation of the effective aerial degrees of freedom of the ESPARs is also discussed. Two simulation examples of ESPARs, a 4-element linear dipole array and an 8-element rectangular planar inverted-F antenna array, using SM as well as full multiplexed MIMO are provided, demonstrating the effectiveness of the proposed method.**

***Index Terms*— Aerial degrees of freedom, ESPAR, MIMO, orthogonal pattern, space modulation, theory of characteristic modes.**

I. Introduction

MULTIPLE-input multiple-output (MIMO) systems play a critical role in enhancing the spectral efficiency (SE) of wireless communication systems [1], [2]. However, energy efficiency (EE) has also become an important parameter and tradeoffs between SE and EE have become necessary as communication system complexity increases [3], [4]. One approach to performing this tradeoff is using hybrid precoding and a variety of techniques and methods have been proposed [5], [6] including the use of highly reconfigurable antennas [7]. Another approach that has been proposed is to use single-radio-frequency (RF) MIMO communication [8], [9] and the conventional technique to exploit this architecture is to use space modulation (SM) [10], [11]. SM offers an increase of EE but at the expense of SE and the spatial diversity required for SM is often formed through switching the feeds of spatially separated antennas.

Electronically Steerable Passive Array Radiator (ESPAR) antennas have also been utilized to provide single-RF MIMO systems by switching between radiation patterns [8], [12]–[14]. Mutual coupling between the single active element and the parasitic elements in ESPAR is harnessed to form the required orthogonal patterns through switched parasitic element loads [15]. ESPAR has been utilized in both SM and full multiplexed MIMO using modulation schemes such as ON-OFF keying (OOK), phase shift keying (PSK) and 16-QAM [16]–[18]. Channel estimation techniques for ESPAR have also been proposed [19] and investigations into the effect of quantized or switched loads have been performed [20]. The use of switched parasitic loading to create benefits has also been leveraged in other contexts such as overcoming reductions in capacity resulting from mutual coupling [21], [22]. ESPAR has also been applied to frequency-selective channels by using orthogonal frequency division multiplexing (OFDM), but the number of switched loads needs to be increased as compared to frequency flat channel configurations [23]. Utilizing single-carrier broadband transmission for handling frequency-selective channels, such as frequency domain equalization (SC-FDE) [24], [25], would also be possible using ESPAR. The development of ESPAR has also resulted in antenna designs to support single-RF MIMO systems [26]–[28].

To analyze the performance of ESPAR single-RF MIMO systems, the concept of the beamspace domain is often used [8], [29], [30]. The beamspace domain interprets the formation of MIMO sub-channels by associating them with a corresponding orthogonal beam or pattern. In essence the orthogonal beams form independent sub-channels in a similar way to the spatial separation of antennas that form spatial sub-channels. When ESPAR is interpreted in the beamspace domain both SM and full multiplexed single-RF MIMO systems can be analyzed [31]–[33].

Manuscript received May 10, 2020; revised September 15, 2020 and November 26, 2020; accepted November 26, 2020. Date of publication December 8, 2020; date of current version April 9, 2021. This work was supported by the Hong Kong research councils General Research Fund under Grant 16208117 and Grant 16209019. The associate editor coordinating the review of this article and approving it for publication was R. Dinis. *(Corresponding author: Shanpu Shen.)*

Zixiang Han, Yujie Zhang, Shanpu Shen, Yue Li, and Chi-Yuk Chiu are with the Department of Electronic and Computer Engineering, The Hong Kong University of Science and Technology, Kowloon, Hong Kong (e-mail: sshenaa@connect.ust.hk).

Ross Murch is with the Department of Electronic and Computer Engineering, Institute for Advanced Study, The Hong Kong University of Science and Technology, Kowloon, Hong Kong.

There are several challenges in creating suitable ESPAR systems to support full spatial multiplexing single-RF MIMO. The first of these is their typically narrow bandwidth due to the mutual coupling needed for an ESPAR. Methods to overcome this include the careful design of the parasitic elements so that the mutual coupling is neither too high or low. Alternatives to overcome the bandwidth issue such as load modulated arrays (LMA) have also been proposed but still in development [34], [35]. Furthermore, it is also challenging to maintain good impedance matching across the different patterns in ESPAR. This can be overcome by switching tunable matching networks consisting of switched transmission lines (TLs) [35], [36] or lumped elements [37]. The main disadvantage of this approach is increased insertion loss but this can be kept low by using low loss substrate and PIN diodes to construct tunable TL networks [36].

A key challenge in designing ESPAR to support single-RF MIMO is constructing the required orthogonal far-field patterns in ESPAR. This is not straightforward and is dependent on intuition regarding the specific parasitic antenna configuration [8], [33], [38]. The Gram-Schmidt orthonormalization (GSO) procedure has been used to overcome this drawback to find an orthonormal basis set for the patterns [31]. Using the GSO approach the concept of aerial degrees-of-freedom (ADoF) has also been introduced. ADoF provides an estimate of the number of basis functions a given ESPAR can provide [32]. The GSO approach is useful for certain canonical antenna element types, such as dipoles, which have analytical far-field pattern expressions. However, for other antenna types it can only be applied numerically and does not leverage any of the underlying electromagnetic properties of ESPAR. For this reason ESPAR has been mainly restricted to antennas based on dipole elements limiting its use. In addition the method to find the optimal load reactances in these methods is usually performed by exhaustive search [15] which is also not efficient when the number of parasitic antennas becomes large.

In this article we describe a systematic method for finding the orthonormal radiation patterns required for ESPAR as well as the necessary parasitic load reactances to produce those patterns. The method is based on the Theory of Characteristic Mode (TCM) [39]–[41]. In particular, an N-port TCM formulation has been proposed in 1973 [42]–[44], which has also been recently applied to pixel antenna optimization [45]. The specific contributions of this work are:

1) We apply N-port TCM to obtain orthonormal patterns for use in an ESPAR antenna with only one feeding element and $N-1$ parasitic elements. The approach is general and is not restricted to antenna type or array configuration.

2) We provide closed form solutions, using N-port TCM, for the antenna element currents that produce the required N orthogonal patterns for rectangular, circular, and linear array configurations with arbitrary antenna type.

3) We characterize the antenna coupling within ESPAR through the condition number of a mode matrix. We also investigate the relationship between the condition number, element separation, and effective ADoF through numerical simulations, providing a guide on how to construct efficient ESPAR with proper element separation.

4) We provide an efficient optimization method based on the quasi-Newton method for finding the optimal load reactances to excite the required N orthogonal patterns with only one feeding element. We also provide a closed form expression for an initial approximate solution. The proposed optimization method is more effective than exhaustive search methods used previously.

5) We simulate, using full electromagnetic simulation software, the orthogonal patterns for a 4-element uniform linear dipole array and an 8-element rectangular planar inverted-F antenna (PIFA) array using the proposed methods. Simulation results including SE, EE and symbol error rate (SER) for SM-MISO and full multiplexed MIMO systems are provided and demonstrate the feasibility of using TCM to implement ESPAR for single-RF MIMO.

Organization: Section II introduces N-port TCM. The analysis for various ESPAR configurations using N-port TCM is presented in Section III. In addition the mode matrix condition number is introduced as well as its relation to ADoF. Section IV describes a method to efficiently determine the required reactance loads. In Section V, we introduce two example ESPAR designs and the associated patterns and loads using our approach and provide numerical results for EE, SE and SER to demonstrate the feasibility of the approach. Section VI concludes the work.

Notation: Bold lower and upper case letters denote vectors and matrices respectively, and letters not in bold font represent scalars. $\mathfrak{Re}\{a\}$, $\mathfrak{Im}\{a\}$, and $|a|$ refer to the real part, imaginary part, and modulus of a complex scalar a, respectively. $[\mathbf{a}]_i$ and $\|\mathbf{a}\|$ refer to the ith element and l_2-norm of vector $\mathbf{a}$, respectively. $\mathbf{A}^T$, $\mathbf{A}^H$,$[\mathbf{A}]_i$, $[\mathbf{A}]_{ij}$, and $\det(\mathbf{A})$ refer to the transpose, conjugate transpose, ith row, (i,j)th element, and determinant of a matrix $\mathbf{A}$, respectively. $\mathbb{R}$ and $\mathbb{C}$ denote real and complex number sets respectively and $j=\sqrt{-1}$ denotes an imaginary number. $\mathcal{CN}(\mu,\sigma^2)$ denotes complex Gaussian distribution with mean μ and variance σ^2. $\mathbf{0}_N$ denotes an N-dimensional zero column vector and $\mathbf{0}_{M\times N}$ denotes a $M\times N$ zero matrix. $\mathbf{U}_N$ denotes an $N\times N$ identity matrix. $\text{diag}(a_1,\ldots,a_N)$ is a diagonal matrix with elements being $a_1,\ldots,a_N$ while $\text{diag}(\mathbf{A}_1,\ldots,\mathbf{A}_N)$ is a block diagonal matrix with its matrix elements being $\mathbf{A}_1,\ldots,\mathbf{A}_N$.

II. N-Port Characteristic Mode Analysis

Consider an arbitrary N-port antenna system (N multiple antennas) with the nth port loaded with a reactance x_n^L as shown in Fig. 1. The nth port is excited by a voltage source v_n and the resultant current through the nth port is denoted as i_n. We group v_n and i_n $(n=1,\ldots,N)$ into vectors as $\mathbf{v}=[v_1,v_2,\ldots,v_N]^T$ and $\mathbf{i}=[i_1,i_2,\ldots,i_N]^T$ and they are related by

$$\mathbf{v}=\left(\mathbf{Z}+\mathbf{X}^L\right)\mathbf{i} \tag{1}$$

where $\mathbf{Z}$ denotes the impedance matrix of the N-port antenna and $\mathbf{X}^L$ is a diagonal matrix defined by $\mathbf{X}^L=\text{diag}\left(x_1^L,x_2^L,\cdots,x_N^L\right)$ which represents the load reactance connected to each port. The antenna impedance matrix $\mathbf{Z}$ is complex symmetric where $[\mathbf{Z}]_{ii}$ refers to the self-impedance of

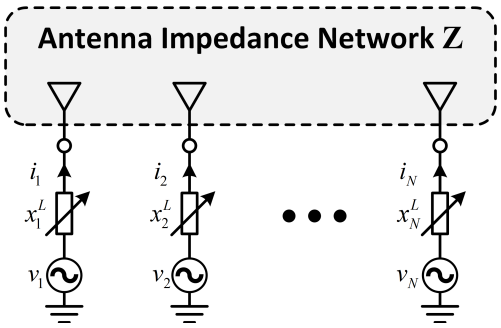

Fig. 1. N-port antenna system loaded with reactances and voltage sources.

the ith port and $[\mathbf{Z}]_{ij} = [\mathbf{Z}]_{ji}$ refers to the mutual impedance between the ith and jth port. We also use $\mathbf{R} = \Re\mathfrak{e}\{\mathbf{Z}\}$ to denote the antenna resistance matrix and $\mathbf{X} = \Im\mathfrak{m}\{\mathbf{Z}\}$ to denote the antenna reactance matrix so that $\mathbf{Z} = \mathbf{R} + j\mathbf{X}$. In all these expressions the dependence of all variables on frequency is assumed and it is not explicitly shown for brevity.

The N-port characteristic modes can be defined by the weighted eigenvalue problem [42]

$$\mathbf{Z}\mathbf{i}_n = (1 + j\lambda_n)\,\mathbf{R}\mathbf{i}_n \tag{2}$$

where $\mathbf{i}_n$ is the eigenvector or modal current and $(1 + j\lambda_n)$ is the eigenvalue for the nth mode. The concept behind (2) is that at a given frequency, every conducting object (such as an antenna system) has a particular set of surface currents and corresponding radiated far-fields associated with it. These are characteristics of the objects shape and independent of any specific excitation [40], [46]. If one of the resulting characteristic modal radiated far-fields is used to excite the object, the scattered radiation will have exactly the same far-field pattern and its magnitude will be related to the eigenvalue of that characteristic mode (CM) [40], [45], [46]. Therefore, TCM offers insights into the natural resonant phenomena of any antenna system including ESPAR.

Substituting $\mathbf{Z} = \mathbf{R} + \mathrm{j}\mathbf{X}$ into (2), we have

$$\mathbf{X}\mathbf{i}_n = \lambda_n \mathbf{R}\mathbf{i}_n \tag{3}$$

which is a real symmetric eigenvalue problem so the eigenvalue λ_n and the eigenvector $\mathbf{i}_n$ for the nth mode are both real. Excited by the nth modal current $\mathbf{i}_n$, the nth modal radiation pattern $\mathbf{e}_n(\Omega)$ is given by

$$\mathbf{e}_n(\Omega) = \sum_{i=1}^{N} [\mathbf{i}_n]_i \, \mathbf{e}_i^{\mathrm{oc}}(\Omega) \tag{4}$$

where $\Omega = (\theta, \phi)$ denotes the spatial angle in which θ and ϕ represent the elevation and azimuth angles in spherical coordinates, and $\mathbf{e}_i^{\mathrm{oc}}(\Omega)$ denotes the radiation pattern of the ith antenna port excited by a unit current when all the other antenna ports are open [42].

A. Orthogonal Modal Current and Pattern

Characteristic modes are orthogonal to each other [42]. In particular the orthogonality of modal currents can be expressed as [42]

$$\mathbf{i}_m^T \mathbf{R}\mathbf{i}_n = \delta_{mn} \tag{5}$$

where δ_{mn} is the Kronecker delta function (0 if $m \neq n$ and 1 if $m = n$) and the orthogonality of $\mathbf{i}_n$ is weighted by $\mathbf{R}$. Importantly, the modal radiation patterns are also orthogonal so that

$$\frac{1}{\eta} \oiint_{S_\infty} \mathbf{e}_m^H(\Omega)\, \mathbf{e}_n(\Omega)\, \mathrm{d}s = \delta_{mn} \tag{6}$$

where η is intrinsic impedance of free space and S_∞ is the surface of a sphere enclosing ESPAR in the far-field [44]. The specific antenna geometry or its ground plane dimensions does not affect the applicability of TCM and the orthogonality properties of (5) and (6) always hold.

The orthogonal modal radiation pattern $\mathbf{e}_n(\Omega)$ found by characteristic mode analysis provides an efficient approach to find an orthogonal basis set for the radiation patterns of any N-port antenna including ESPAR. Specifically, any current vector $\mathbf{i}$ can be written as a linear combination of the modal currents

$$\mathbf{i} = \sum_{n=1}^{N} \alpha_n \mathbf{i}_n \tag{7}$$

where α_n is the nth modal weighting coefficients. Accordingly, the radiation pattern excited by the current vector $\mathbf{i}$, denoted as $\mathbf{e}^r(\Omega)$, can be also written as a linear combination of the modal radiation patterns $\mathbf{e}_n(\Omega)$

$$\mathbf{e}^r(\Omega) = \sum_{n=1}^{N} \alpha_n \mathbf{e}_n(\Omega). \tag{8}$$

B. Single Voltage Source Excitation

We can utilize the orthogonal modal radiation patterns (4) directly for SM or full multiplexed MIMO through (8) without having to resort to bespoke solutions for each antenna type and configuration. In particular we only need to excite one port (with the voltage sources of all other ports set to zero), and set the load reactances $\mathbf{X}^L$ of the other ports to produce the desired modal currents and the corresponding orthogonal patterns. This configuration forms an ESPAR that can be utilized in a single-RF MIMO system. More specifically, with reference to Fig. 1, we designate Port 1 as the feeding port with voltage source excitation v_1 to form the ESPAR for the remainder of this article. To radiate the required orthogonal modal patterns we then need to find the required load reactances (which are denoted as $\mathbf{X}_n^L$ in the remainder of this article) that correspond to modal currents $\mathbf{i}_n$ so that $\left(\mathbf{Z} + \mathbf{X}_n^L\right)^{-1}\mathbf{v} = \mathbf{i}_\mathrm{n}$ in which $\mathbf{v} = [v_1, 0, \ldots, 0]^T$ where v_1 represents the ESPAR voltage excitation.

The method for determining $\mathbf{X}_n^L$ is described in Section IV while the eigenvalue and eigenvector properties for specific antenna configurations are described next.

III. Eigenvalue and Eigenvector Properties for Specific Antenna Array Configurations

Utilizing the framework in Section II, it is useful to calculate the properties of the eigenvalues and eigenvectors for specific antenna array configurations such as rectangular, circular and

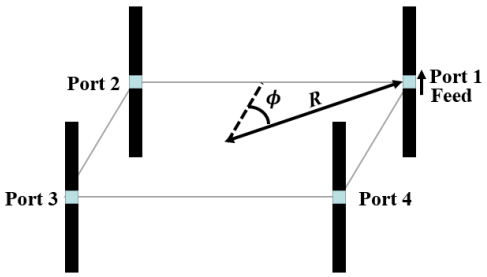

Fig. 2. 4-element rectangular array.

linear arrays. We start by considering 4-element array configurations and then generalize to N-element array configurations. To deduce the properties of the eigenvalues and eigenvectors of specific antenna configurations we rewrite (3) as

$$\mathbf{M}\mathbf{i}_n = \lambda_n \mathbf{i}_n \tag{9}$$

where $\mathbf{M} = \mathbf{R}^{-1}\mathbf{X}$ and it is referred to as the *mode matrix* in the remainder of this article.

To help put the results into context, consider a basic reference antenna array configuration, consisting of N identical uncoupled antennas. For this reference antenna array, $\mathbf{R} = r\mathbf{U}_N$, $\mathbf{X} = x\mathbf{U}_N$, (recall that $\mathbf{U}_N$ is used to denote an $N \times N$ identity matrix) and the mode matrix is given by $\mathbf{M} = x/r\mathbf{U}_N$ (where $r > 0$ and x are arbitrary values). Therefore, the nth eigenvalue is $\lambda_n = x/r$ and the nth eigenvector is the nth column vector of $\mathbf{U}_N$. Because the antennas are uncoupled it cannot be used for ESPAR but it is a useful reference for comparison with the coupled geometries described next.

A. Eigenvectors for Specific Antenna Array Configurations

1) Rectangular Array: Consider a 4-element 2×2 rectangular array by referring to Fig. 2. Utilizing array symmetry we write the mode matrix in a special form (see Appendix A. A)

$$\mathbf{M} = \begin{bmatrix} a & b & c & d \\ b & a & d & c \\ c & d & a & b \\ d & c & b & a \end{bmatrix} \tag{10}$$

where the elements a, b, c, and d are all real scalars for any antenna type and array dimension. (in the special case of a 2×2 square array ($\phi = 45°$) we have $b = d$). Due to the special matrix form, the four eigenvectors are found to be constant vectors (see Appendix A. A) given by

$$\mathbf{i}_1 = \begin{bmatrix} 0.5 \\ 0.5 \\ 0.5 \\ 0.5 \end{bmatrix}, \mathbf{i}_2 = \begin{bmatrix} 0.5 \\ -0.5 \\ -0.5 \\ 0.5 \end{bmatrix}, \mathbf{i}_3 = \begin{bmatrix} 0.5 \\ -0.5 \\ 0.5 \\ -0.5 \end{bmatrix}, \mathbf{i}_4 = \begin{bmatrix} 0.5 \\ 0.5 \\ -0.5 \\ -0.5 \end{bmatrix}, \tag{11}$$

where the norm of each eigenvector is normalized to unity without loss of generality (and is performed in all the examples that follow). The first entry of each eigenvector corresponds to the current through Port 1. All entries in (11) have the same magnitude $|[\mathbf{i}_n]_i| = 0.5$ for n, $i = 1, 2, 3, 4$, so that each antenna contributes equally to the modal patterns (4) no matter the geometry dimensions or antenna type.

We can generalize the form (10) by nesting four identical $p \times q$ arrays into the element positions of the original 2×2 array forming a clustered $2p \times 2q$-element array. The elements a, b, c, and d in (10) are replaced by matrices $\mathbf{A}$, $\mathbf{B}$, $\mathbf{C}$, and $\mathbf{D} \in \mathbb{R}^{pq \times pq}$. The eigenvectors of the $2p \times 2q$-element array have a special structure (see Appendix A. A) and the $4pq$ eigenvectors have the forms

$$\mathbf{i}_{1,n} = \begin{bmatrix} \tilde{\mathbf{i}}_{1,n} \\ \tilde{\mathbf{i}}_{1,n} \\ \tilde{\mathbf{i}}_{1,n} \\ \tilde{\mathbf{i}}_{1,n} \end{bmatrix}, \mathbf{i}_{2,n} = \begin{bmatrix} \tilde{\mathbf{i}}_{2,n} \\ -\tilde{\mathbf{i}}_{2,n} \\ -\tilde{\mathbf{i}}_{2,n} \\ \tilde{\mathbf{i}}_{2,n} \end{bmatrix},$$
$$\mathbf{i}_{3,n} = \begin{bmatrix} \tilde{\mathbf{i}}_{3,n} \\ -\tilde{\mathbf{i}}_{3,n} \\ \tilde{\mathbf{i}}_{3,n} \\ -\tilde{\mathbf{i}}_{3,n} \end{bmatrix}, \mathbf{i}_{4,n} = \begin{bmatrix} \tilde{\mathbf{i}}_{4,n} \\ \tilde{\mathbf{i}}_{4,n} \\ -\tilde{\mathbf{i}}_{4,n} \\ -\tilde{\mathbf{i}}_{4,n} \end{bmatrix}, \tag{12}$$

for $n = 1, 2, \ldots, pq$ and where $\tilde{\mathbf{i}}_{1,n}, \tilde{\mathbf{i}}_{2,n}, \tilde{\mathbf{i}}_{3,n}$, and $\tilde{\mathbf{i}}_{4,n} \in \mathbb{R}^{pq \times 1}$ are eigenvectors of matrices $\mathbf{A} + \mathbf{B} + \mathbf{C} + \mathbf{D}$, $\mathbf{A} - \mathbf{B} - \mathbf{C} + \mathbf{D}$, $\mathbf{A} - \mathbf{B} + \mathbf{C} - \mathbf{D}$ and $\mathbf{A} + \mathbf{B} - \mathbf{C} - \mathbf{D}$ respectively, but are normalized so that $\left\|\tilde{\mathbf{i}}_{m,n}\right\| = 0.5$ for $m = 1, 2, 3, 4$ and $n = 1, 2, \ldots, pq$. For each of the eigenvectors $\mathbf{i}_{m,n}$, $m = 1, 2, 3, 4$, it consists of four identical sub-eigenvectors $\tilde{\mathbf{i}}_{m,n}$ with different signs. Hence, in total $4pq$ eigenvectors are formed. It is useful to note that the norm of each of the $\tilde{\mathbf{i}}_{m,n}$ are the same so that each $p \times q$ sub-array contributes equally to the modal patterns.

For $m \times n$ rectangular arrays where either m or n is odd, such as 3×2 or 3×3 configurations, we can treat them as linear arrays and for example three sub-arrays each with 2 or 3 elements. This extension is briefly described at the end of Section III. A. 3.

In Section IV we provide results for an 8-element rectangular array ESPAR using PIFAs which is formed by putting clusters of 1×2 identical arrays into an 2×2 array forming a clustered 2×4-element array with 8 eigenvectors. The 8 eigenvectors, $\mathbf{i}_{1,n}$, $\mathbf{i}_{2,n}$, $\mathbf{i}_{3,n}$, and $\mathbf{i}_{4,n}$ for $n = 1$ and 2, provided by (12), will be formed as shown in Section IV.

2) Circular Array With Center Feeding: Conventionally ESPAR is configured as a circular array with a feeding port in the center as shown in Fig. 3. In the configuration in Fig. 3, $\mathbf{M}$ can be written as (see Appendix A. B)

$$\mathbf{M} = \begin{bmatrix} a & b & b & b & b \\ c & d & e & f & e \\ c & e & d & e & f \\ c & f & e & d & e \\ c & e & f & e & d \end{bmatrix} \tag{13}$$

where a, b, c, d, e, and f are real scalars. Five eigenvectors of $\mathbf{M}$ are (see Appendix A. B)

$$\mathbf{i}_1 = \frac{1}{\sqrt{1+4\alpha_1^2}} \begin{bmatrix} 1 \\ \alpha_1 \\ \alpha_1 \\ \alpha_1 \\ \alpha_1 \end{bmatrix}, \mathbf{i}_2 = \frac{1}{\sqrt{1+4\alpha_2^2}} \begin{bmatrix} 1 \\ \alpha_2 \\ \alpha_2 \\ \alpha_2 \\ \alpha_2 \end{bmatrix},$$

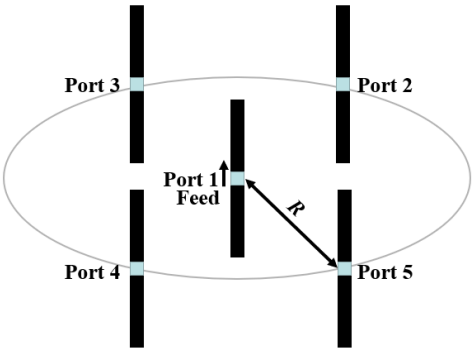

Fig. 3. 5-element circular array with center feeding.

$$\mathbf{i}_3 = \begin{bmatrix} 0 \\ 0.5 \\ -0.5 \\ 0.5 \\ -0.5 \end{bmatrix}, \mathbf{i}_4 = \begin{bmatrix} 0 \\ 0 \\ -\frac{1}{\sqrt{2}} \\ 0 \\ \frac{1}{\sqrt{2}} \end{bmatrix}, \mathbf{i}_5 = \begin{bmatrix} 0 \\ -\frac{1}{\sqrt{2}} \\ 0 \\ \frac{1}{\sqrt{2}} \\ 0 \end{bmatrix}, \tag{14}$$

where α_1 and α_2 are given by

$$\alpha_{1,2} = \frac{(d+2e+f-a) \pm \sqrt{(d+2e+f-a)^2+16bc}}{8b}. \tag{15}$$

Zero entries in eigenvectors imply the corresponding ports should be open (zero current). When a zero entry occurs at the feeding element (Port 1) such as currents $\mathbf{i}_3$, $\mathbf{i}_4$, and $\mathbf{i}_5$ in (14), it indicates that Port 1 has to be open if we want to excite the corresponding modal radiation pattern. However, this contradicts the ESPAR required that we only excite Port 1 in a single source configuration. Therefore, for a single voltage source excitation this result is not satisfactory as feed Port 1 cannot be set to zero.

To solve the single port excitation problem we can rotate the orthogonal pattern basis to achieve a new orthogonal pattern basis. For example, in this 5-element circular array configuration, we can utilize a matrix for the 5 modal radiation patterns, $\mathbf{E}_5 = \left[\mathbf{e}_1, \mathbf{e}_2, \mathbf{e}_3, \mathbf{e}_4, \mathbf{e}_5\right]$ so that $\mathbf{E}_5$ satisfies $\frac{1}{\eta}\oiint_{S_\infty} \mathbf{E}_5^H \mathbf{E}_5 \, \mathrm{d}s = \mathbf{U}_5$. A unitary matrix $\mathbf{T} \in \mathbb{C}^{5\times 5}$ can then be used to rotate the orthogonal pattern basis where $[\mathbf{T}]_1$ should not contain a zero entry to ensure that modal pattern $\mathbf{e}_1$ is mixed with other modal patterns. The new basis obtained can be written as $\tilde{\mathbf{E}}_5 = \mathbf{E}_5\mathbf{T} = \left[\tilde{\mathbf{e}}_1, \tilde{\mathbf{e}}_2, \tilde{\mathbf{e}}_3, \tilde{\mathbf{e}}_4, \tilde{\mathbf{e}}_5\right]$, which is also an orthogonal basis since

$$\begin{aligned} \frac{1}{\eta}\oiint_{S_\infty} \tilde{\mathbf{E}}_5^H \tilde{\mathbf{E}}_5 \, \mathrm{d}s &= \mathbf{T}^H \left(\frac{1}{\eta}\oiint_{S_\infty} \mathbf{E}_5^H \mathbf{E}_5 \, \mathrm{d}s\right) \mathbf{T} \\ &= \mathbf{T}^H \mathbf{U}_5 \mathbf{T} = \mathbf{U}_5. \end{aligned} \tag{16}$$

The corresponding modal currents can also be found by utilizing a unitary matrix for the 5 eigenvectors, $\mathbf{I}_5 = \left[\mathbf{i}_1, \mathbf{i}_2, \mathbf{i}_3, \mathbf{i}_4, \mathbf{i}_5\right]$, so that after rotation the new currents become $\tilde{\mathbf{I}}_5 = \mathbf{I}_5\mathbf{T}$. Therefore the first entries of the current vectors are non-zero because $\mathbf{i}_1$ is mixed with $\mathbf{i}_2$, $\mathbf{i}_3$, $\mathbf{i}_4$ and $\mathbf{i}_5$. As a result we can excite the rotated current vectors to generate orthogonal radiation patterns with a single voltage source at the feeding element Port 1.

We can also generalize the circular array form to N elements. We restrict the configuration to odd numbers of elements [8], [16] so there is one feeding element in the center and an even number of parasitic elements are uniformly spaced around the circle. We divide the parasitic elements into two identical groups each with $\frac{N-1}{2}$ elements, e.g. in Fig. 3 we can choose Ports 2 and 3 as a group and Ports 4 and 5 as the other group so that two groups are symmetrical about the feeding element. The mode matrix can then be written as

$$\mathbf{M} = \begin{bmatrix} a & \mathbf{b} & \mathbf{b} \\ \mathbf{c} & \mathbf{D} & \mathbf{E} \\ \mathbf{c} & \mathbf{E} & \mathbf{D} \end{bmatrix} \tag{17}$$

where a is scalar, $\mathbf{b} \in \mathbb{R}^{1\times\frac{N-1}{2}}$, $\mathbf{c} \in \mathbb{R}^{\frac{N-1}{2}\times 1}$, $\mathbf{D}, \mathbf{E} \in \mathbb{R}^{\frac{N-1}{2}\times\frac{N-1}{2}}$. The N eigenvectors can be classified into two forms (see Appendix A. B)

$$\mathbf{i}_{1,n} = \begin{bmatrix} i_{1,n} \\ \tilde{\mathbf{i}}_{1,n} \\ \tilde{\mathbf{i}}_{1,n} \end{bmatrix}, \quad \mathbf{i}_{2,n} = \begin{bmatrix} 0 \\ \tilde{\mathbf{i}}_{2,n} \\ -\tilde{\mathbf{i}}_{2,n} \end{bmatrix}, \tag{18}$$

where $i_{1,n}$ is a scalar and $\tilde{\mathbf{i}}_{1,n}$, $\tilde{\mathbf{i}}_{2,n} \in \mathbb{R}^{\frac{N-1}{2}\times 1}$. $\tilde{\mathbf{i}}_{2,n}$ are eigenvectors of $\mathbf{D}-\mathbf{E}$ and normalized to $\left\|\tilde{\mathbf{i}}_{2,n}\right\| = \frac{1}{\sqrt{2}}$ for $n = 1, 2, \ldots, \frac{N-1}{2}$ while $i_{1,n}$ and $\tilde{\mathbf{i}}_{1,n}$ are related to a, $\mathbf{b}$, $\mathbf{c}$, $\mathbf{D}$, $\mathbf{E}$ and we have $\|\mathbf{i}_{1,n}\| = 1$ for $n = 1, 2, \ldots \frac{N+1}{2}$. That is $\frac{N+1}{2}$ eigenvectors take the form of $\mathbf{i}_{1,n}$ and the other $\frac{N-1}{2}$ eigenvectors have the form $\mathbf{i}_{2,n}$. There is at least one eigenvector containing a zero at Port 1. We can rotate the orthogonal pattern basis, as previously described, to solve this problem.

3) Linear Array: The last considered configuration is a 4-element linear array as Fig. 4 shows.

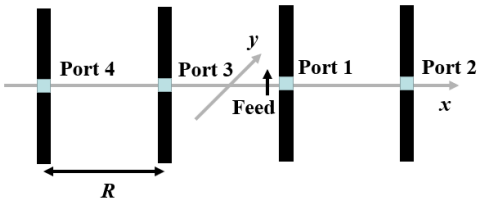

Fig. 4. 4-element linear array.

This structure is not as straightforward as the previous arrays and the mode matrix can be written as (see Appendix A. C)

$$\mathbf{M} = \begin{bmatrix} a & b & c & d \\ e & f & g & h \\ c & d & a & b \\ g & h & e & f \end{bmatrix}. \tag{19}$$

The four eigenvectors can be written generally as (see Appendix A. C)

$$\begin{aligned} \mathbf{i}_1 &= \frac{1}{\sqrt{2+2\alpha_1^2}} \begin{bmatrix} 1 \\ \alpha_1 \\ 1 \\ \alpha_1 \end{bmatrix}, \mathbf{i}_2 = \frac{1}{\sqrt{2+2\alpha_2^2}} \begin{bmatrix} 1 \\ \alpha_2 \\ 1 \\ \alpha_2 \end{bmatrix}, \\ \mathbf{i}_3 &= \frac{1}{\sqrt{2+2\alpha_3^2}} \begin{bmatrix} 1 \\ \alpha_3 \\ -1 \\ -\alpha_3 \end{bmatrix}, \mathbf{i}_4 = \frac{1}{\sqrt{2+2\alpha_4^2}} \begin{bmatrix} 1 \\ \alpha_4 \\ -1 \\ -\alpha_4 \end{bmatrix}, \end{aligned} \tag{20}$$

where α_1, α_2, α_3, and α_4 are given by

$$\alpha_{1,2} = \frac{f+h-a-c}{2\left(b+d\right)} \pm \sqrt{\frac{\left(f+h-a-c\right)^2}{4\left(b+d\right)^2} + \frac{e+g}{b+d}}, \tag{21}$$

$$\alpha_{3,4} = \frac{f-h-a+c}{2\left(b-d\right)} \pm \sqrt{\frac{\left(f-h-a+c\right)^2}{4\left(b-d\right)^2} + \frac{e-g}{b-d}}. \tag{22}$$

This structure is good since all the elements of all eigenvectors are non-zero. However if $b = d$ or $e = g$ then $x = 0$ but this is an unlikely occurrence.

Generalizing the linear array to an arbitrary number of elements can be performed separately for odd and even element numbers. For odd numbers of elements, two identical subarrays are placed at each side of a center feeding element, so the analysis is the same as Section III. A. 2. For even numbers, as in Fig. (4), Port 3 is the opposite element of the feeding element, Port 1. Then there are two identical groups of elements at left and right hand sides that can be treated as two subarrays such that

$$\mathbf{M} = \begin{bmatrix} a & \mathbf{b} & c & \mathbf{d} \\ \mathbf{e} & \mathbf{F} & \mathbf{g} & \mathbf{H} \\ c & \mathbf{d} & a & \mathbf{b} \\ \mathbf{g} & \mathbf{H} & \mathbf{e} & \mathbf{F} \end{bmatrix} \tag{23}$$

where a and c are scalars, $\mathbf{b}, \mathbf{d} \in \mathbb{R}^{1\times(\frac{N}{2}-1)}$, $\mathbf{e}, \mathbf{g} \in \mathbb{R}^{(\frac{N}{2}-1)\times 1}$, and $\mathbf{F}$, $\mathbf{H} \in \mathbb{R}^{(\frac{N}{2}-1)\times(\frac{N}{2}-1)}$. The N eigenvectors have two common forms (see Appendix A. C) each with $\frac{N}{2}$ different eigenvectors

$$\mathbf{i}_{1,n} = \begin{bmatrix} \tilde{\mathbf{i}}_{1,n} \\ \tilde{\mathbf{i}}_{1,n} \end{bmatrix}, \mathbf{i}_{2,n} = \begin{bmatrix} \tilde{\mathbf{i}}_{2,n} \\ -\tilde{\mathbf{i}}_{2,n} \end{bmatrix}, \tag{24}$$

where $\tilde{\mathbf{i}}_{1,n}, \tilde{\mathbf{i}}_{2,n} \in \mathbb{R}^{\frac{N}{2}\times 1}$, $\left\|\tilde{\mathbf{i}}_{1,n}\right\| = \left\|\tilde{\mathbf{i}}_{2,n}\right\| = \frac{1}{\sqrt{2}}$ for $n = 1, 2, \ldots, \frac{N}{2}$.

Further generalization of the linear array can be performed by replacing each element with a sub-array and this can be used to handle $m \times n$ rectangular arrays where either m or n is odd. For example we can regard a rectangular array as a linear array consisting of m (or n) sub-arrays each with n (or m) elements. In particular, for a 3×2 array or a 3×3 array, we can treat them as linear arrays with three sub-arrays each with 2 or 3 elements. The analysis is same as the odd element number version of linear array described above, with the only difference being element a in (17) becomes a matrix $\mathbf{A}$ since more than one element is in the center sub-array.

In Section IV we provide results for a 4-element linear array ESPAR using dipole antennas.

B. Eigenvalues

For an uncoupled antenna array with identical antennas all the eigenvalues are equal. However, for coupled antenna arrays the eigenvalues will no longer be all equal. To estimate the antenna coupling within ESPAR, when all antenna elements are identical and matched, we use the condition number of the mode matrix $\mathbf{M}$, denoted as κ and given by

$$\kappa = \frac{\max\limits_{n=1,\ldots,N} |\lambda_n|}{\min\limits_{n=1,\ldots,N} |\lambda_n|}. \tag{25}$$

The condition number is the ratio between the highest and lowest absolute values of the eigenvalues of the mode matrix $\mathbf{M}$ [47].

The condition number κ is always greater than or equal to unity. If κ is unity, there is no coupling as shown in the reference example of an uncoupled antenna array with identical antennas. Accordingly, if κ is close to unity, the coupling becomes negligible. In this situation, changing the load on one antenna port will not affect the currents on the other ports, so it is not suitable for ESPAR. Therefore, we need to set a constraint for the lower bound on κ to ensure enough coupling for use in ESPAR. We have found through numerical simulation that the condition number κ should be greater than 10 for effective ESPAR and set the lower bound to $\kappa_l = 10$. On the other hand, if the condition number κ is extremely high it implies that $\mathbf{M}$ is close to singular [47] which indicates that some rows of $\mathbf{M}$ are close to being linearly dependent. From the perspective of an antenna array, it implies that the antennas are highly coupled and are close together. In addition, because the condition number κ is high, it also implies that any small changes to the load reactance $\mathbf{X}^L$ in the ESPAR antenna will cause large changes to the current and pattern. This makes the system very sensitive and prone to errors through component tolerances. Therefore, we need to set a constraint for the upper bound on κ to avoid the sensitivity issue. We have found through numerical simulation that κ in practice should be less than 10^4 and set the upper bound $\kappa_u = 10^4$.

The condition numbers for the 4-element rectangular array, 4-element linear array, and 5-element circular array versus element separation are shown in Fig. 5. The element separation is defined as R/λ where R is shown in Figs. 2, 3, 4 and λ is wavelength. From Fig. 5, we find that the condition number decreases as the element separation increases. When the element separation is large, the condition number is small. For example, when $R > 0.5\lambda$, the condition numbers for the 4-element arrays are less than 10 ($\kappa < 10$) while the 5-element circular array has a slightly larger condition number (indicating stronger coupling) but is still less than 50 ($\kappa < 50$). On the other hand, when the element separation is small, the condition number becomes large and the coupling is strong. For those modes whose absolute value of eigenvalues is larger than $\kappa_u \min\limits_{n=1,\ldots,N} |\lambda_n|$, it is difficult to excite them due to the sensitivity to the load values. We also find that the condition number of the rectangular array is smaller than the linear and circular array with center feeding when element separation is small, indicating that elements in the rectangular array should be closer to maintain coupling for mode excitation in ESPAR.

We also consider the effective ADoF (EADoF) in the ESPAR with different element separations and condition numbers. EADoF has been defined in previous work [32] as a measure of the effective number of aerial dimensions of the ESPAR. Using the definition in [32] we plot the estimated

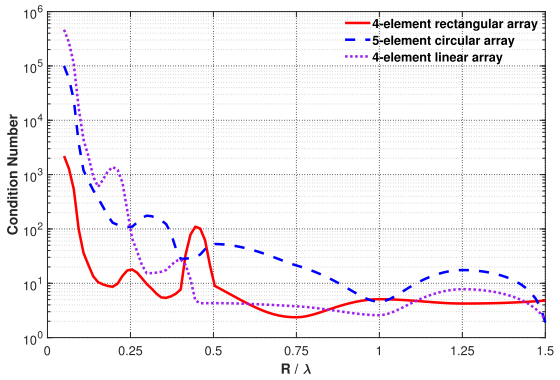

Fig. 5. Condition number versus element separation for different antenna array configurations.

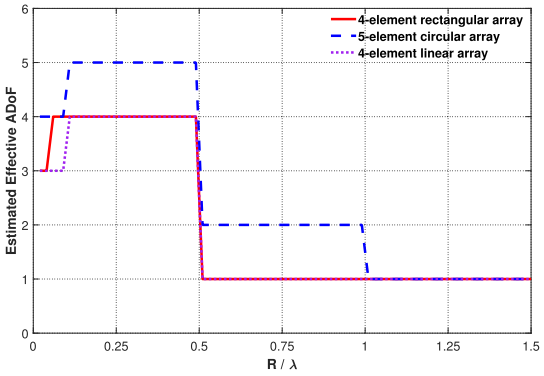

Fig. 6. Effective ADoF versus element separation for different array configurations.

EADoF versus element separation in Fig. 6 for the three array configurations considered. From Fig. 6, we can find that EADoF has a close relationship with the element separation. Therefore, with the results in Fig. 5, we can deduce that EADoF also has a close relationship with the condition number. When κ is approximately less than $\kappa_l = 10$ (e.g. a large separation $R > \lambda$), EADoF reduces to 1. This is because when the separation is large, the antenna coupling is weak, so that the radiation pattern always remains the same whatever the load reactances are. As a result, the combination of modal patterns also remain constant so that the EADoF becomes unity. When κ is approximately larger than $\kappa_u = 10^4$ (e.g. a small separation $R < 0.1\lambda$), there is at least one EADoF loss due to the load sensitivity issue in the highly coupled ESPAR. The EADoF loss can be estimated by counting the number of eigenvalues whose absolute values are greater than $\kappa_u \min\limits_{n=1,\ldots,N} |\lambda_n|$. In general, if $\kappa_l \leq \kappa \leq \kappa_u$ and $0.1\lambda \leq R < 0.5\lambda$, then EADoF will be N without any loss in all these examples.

IV. Load Reactance Optimization

A. Formulation

Given the desired orthogonal modal radiation pattern $\mathbf{e}_n(\Omega)$, we need to find the corresponding load reactances $\mathbf{X}_n^L$ with a given single voltage source at the feeding port (Port 1) to excite the modal current $\mathbf{i}_n$ and subsequently radiate the desired modal pattern. That is, we aim to find $\mathbf{X}_n^L$ so that the radiation pattern produced by $\mathbf{X}_n^L$, which is denoted as $\mathbf{e}^r\left(\Omega, \mathbf{X}_n^L\right)$ and given by

$$\mathbf{e}^r\left(\Omega, \mathbf{X}_n^L\right) = \sum_{i=1}^{N} \left[\left(\mathbf{Z} + \mathbf{X}_n^L\right)^{-1} \mathbf{v}\right]_i \mathbf{e}_i^{\text{oc}}(\Omega), \tag{26}$$

is close to $\mathbf{e}_n(\Omega)$.

To that end, we consider the correlation coefficient between $\mathbf{e}_n(\Omega)$ and $\mathbf{e}^r\left(\Omega, \mathbf{X}_n^L\right)$ defined as

$$\rho_n\left(\mathbf{X}_n^L\right) = \frac{\langle \mathbf{e}_n, \mathbf{e}^r \rangle}{\|\mathbf{e}_n\| \, \|\mathbf{e}^r\|}, \tag{27}$$

where $\langle \mathbf{e}_n, \mathbf{e}^r \rangle$ defines an inner product between $\mathbf{e}_n(\Omega)$ and $\mathbf{e}^r\left(\Omega, \mathbf{X}_n^L\right)$ given by

$$\langle \mathbf{e}_n, \mathbf{e}^r \rangle = \oiint \mathbf{e}_n^H(\Omega)\, \mathbf{e}^r\left(\Omega, \mathbf{X}_n^L\right) \mathrm{d}\Omega, \tag{28}$$

and $\|\mathbf{e}_n\| = \sqrt{\langle \mathbf{e}_n, \mathbf{e}_n \rangle}$ and $\|\mathbf{e}_r\| = \sqrt{\langle \mathbf{e}_r, \mathbf{e}_r \rangle}$ define the norm of $\mathbf{e}_n(\Omega)$ and $\mathbf{e}^r\left(\Omega, \mathbf{X}_n^L\right)$ in the pattern space. The correlation coefficient satisfies $0 \leq \left|\rho_n\left(\mathbf{X}_n^L\right)\right| \leq 1$ and when $\left|\rho_n\left(\mathbf{X}_n^L\right)\right| = 0$, $\mathbf{e}_n(\Omega)$ and $\mathbf{e}^r\left(\Omega, \mathbf{X}_n^L\right)$ are orthogonal. When $\left|\rho_n\left(\mathbf{X}_n^L\right)\right|$ is close to unity, $\mathbf{e}_n(\Omega)$ is very close or the same as $\mathbf{e}^r\left(\Omega, \mathbf{X}_n^L\right)$. Therefore, finding the load reactances $\mathbf{X}_n^L$ to produce the orthogonal modal radiation pattern $\mathbf{e}_n(\Omega)$ can be performed by solving the optimization problem

$$\max_{\mathbf{X}_n^L} \quad \left|\rho_n\left(\mathbf{X}_n^L\right)\right| \tag{29}$$

which aims to make the patterns $\mathbf{e}_n(\Omega)$ and $\mathbf{e}^r\left(\Omega, \mathbf{X}_n^L\right)$ as close to each other as possible.

B. Optimization

The problem (29) is an unconstrained optimization problem. Therefore, efficient optimization algorithms, such as quasi-Newton method [48], can be used to maximize $\rho_n\left(\mathbf{X}_n^L\right)$. However, considering the expression for $\rho_n\left(\mathbf{X}_n^L\right)$, it is difficult to determine the convexity of $\rho_n\left(\mathbf{X}_n^L\right)$. Hence, using the quasi-Newton method could not guarantee convergence to a global optimal solution. Nevertheless, it guarantees convergence to a stationary point of the problem (29).

To help find an optimal solution that is close to the global optimum and support convergence it is important to find a good initial point for the quasi-Newton method. Here we provide a good initial point with closed form solution, based on the relationship between voltage and current within ESPAR systems. In essence we wish to excite the modal current $\mathbf{i}_n$ (so as to radiate the orthogonal pattern $\mathbf{e}_n(\Omega)$) with a single voltage source feeding Port 1 (denoted as $\mathbf{v} = [v_1, 0, \ldots, 0]^T$ where v_1 can be an arbitrary non-zero value that is assumed to be a real number) by tuning the load reactance $\mathbf{X}_n^L$. Therefore, we wish to minimize the difference between $\mathbf{v}$ and $\left(\mathbf{Z} + j\mathbf{X}_n^L\right)\mathbf{i}_n$ (which is the voltage vector excited by the modal current source $\mathbf{i}_n$), so that we can select the initial point $\mathbf{X}_{n,\text{init}}^L$ as

$$\begin{aligned} \mathbf{X}_{n,\text{init}}^L &= \operatorname*{argmin}_{\mathbf{X}_n^L} \left\| \left(\mathbf{R}\mathbf{i}_n - \mathbf{v}\right) + j\left(\mathbf{X} + \mathbf{X}_n^L\right)\mathbf{i}_n \right\| \\ &= \operatorname*{argmin}_{\mathbf{X}_n^L} \left\| \left(\mathbf{Z} + j\mathbf{X}_n^L\right)\mathbf{i}_n - \mathbf{v} \right\|, \end{aligned} \tag{30}$$

where $(\mathbf{R}\mathbf{i}_n - \mathbf{v})$ is the real part and $\left(\mathbf{X} + \mathbf{X}_n^L\right)\mathbf{i}_n$ is the imaginary part ($\mathbf{i}_n$ is a real vector). Because the real part is a constant, $\left\|(\mathbf{R}\mathbf{i}_n - \mathbf{v}) + j\left(\mathbf{X} + \mathbf{X}_n^L\right)\mathbf{i}_n\right\|$ takes the minimum value when the imaginary part is zero. Therefore, $\mathbf{X}_{n,\text{init}}^L$ has a closed form solution given by

$$\left(\mathbf{X} + \mathbf{X}_{n,\text{init}}^L\right)\mathbf{i}_n = \mathbf{0}, \tag{31}$$

which has a unique solution when $\mathbf{X}_{n,\text{init}}^L$ is restricted to being diagonal. The unique solution is given by $\mathbf{X}_{n,\text{init}}^L = \text{diag}\left(x_{n,\text{init},1}^L, x_{n,\text{init},2}^L, \cdots, x_{n,\text{init},N}^L\right)$ with

$$x_{n,\text{init},i}^L = -\frac{[\mathbf{X}\mathbf{i}_n]_i}{[\mathbf{i}_n]_i},\ \forall i. \tag{32}$$

The initial point found by solving (30) can be also interpreted from the perspective of N-port TCM. In N-port TCM, the complex power delivered to the N-port antenna by the nth modal current is $P_n = \mathbf{i}_n^T\mathbf{Z}\mathbf{i}_n = 1 + j\lambda_n$. If λ_n is zero, the driving voltage is in phase with the modal current and the reactive power is zero so that we say this mode is in resonance [42]. If λ_n is nonzero, we can load the reactance $\mathbf{X}_{n,\text{init}}^L$ satisfying (31) to cancel the reactive power so as to make the loaded N-port antenna resonant.

For a voltage source at Port 1 with load reactance $\mathbf{X}_{n,\text{init}}^L$ from (31), we know the nth mode is resonating. However some other modes will also make some contributions to $\mathbf{e}^r$ although they may not be in resonance. We therefore need to further optimize the loads to maximize the correlation coefficient between the modal pattern of interest $\mathbf{e}_n(\Omega)$ and the actual radiation pattern $\mathbf{e}^r\left(\Omega, \mathbf{X}_n^L\right)$. This can be performed by optimization using (31) as the initial solution.

The proposed algorithm can complete optimization normally within a few seconds (on a general purpose personal computer) for all modes. This is more efficient than the exhaustive search approach adopted in [15], particularly when the number of antenna ports is large. This is also more efficient than the random search approach adopted in [32] which generates large amounts of patterns with random load reactance and selects best load reactance that maximizes ρ_n.

The same approach can also be utilized to find linear combinations of the modal radiation patterns to form more intricate pattern constellations that are required in full multiplexed MIMO. For example if we wish to excite the pattern, $\mathbf{e}_n(\Omega) + \mathbf{e}_{n+1}(\Omega)$, the current for which resonance is required is updated to $\mathbf{i} = \mathbf{i}_n + \mathbf{i}_{n+1}$. Using this approach the required load reactance for any constellation point can be found.

Once we have obtained the final optimized solution we also include some post-optimization constraints due to practical component considerations. In particular we constrain the range of load reactance values to within $-j200$ to $j200\ \Omega$ and the resolution of the required inductors and capacitors is limited to 0.1 nH and 0.1 pF. This is performed by taking the final solution and straightforwardly quantizing it to the resolution required. In addition if any reactance falls outside the range $-j200$ to $j200\ \Omega$ it is clipped to within the range. We have found that very few solutions fall outside the range and both post-optimization constraints have little effect on performance as shown in the next section.

TABLE I

EIGENVECTORS AND LOADS OF 4-ELEMENT LINEAR DIPOLE ARRAY AT 2.45GHZ

Eigenvectors	Mode 1	Mode 2	Mode 3	Mode 4
Port 1	-0.66	0.44	0.13	-0.13
Port 2	0.25	-0.55	0.70	-0.70
Port 3	0.66	0.44	0.13	0.13
Port 4	-0.25	-0.55	0.70	0.70
Loads	**Mode 1**	**Mode 2**	**Mode 3**	**Mode 4**
Port 1	5.9 pF	2.3 pF	13.0 nH	0.8 pF
Port 2	12.1 pF	15.6 pF	3.9 nH	0.3 pF
Port 3	5.9 pF	2.3 pF	13.0 nH	6.2 pF
Port 4	12.1 pF	15.6 pF	6.2 nH	2.3 pF

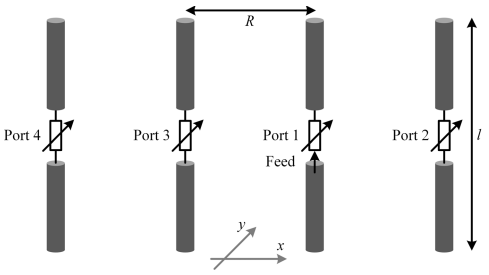

Fig. 7. 4-element linear dipole array.

V. SIMULATION RESULTS

We apply our proposed N-port TCM ESPAR technique to SM-MISO and full multiplexed MIMO and simulation results including SE, EE and SER simulation results are provided to demonstrate its potential. Results are provided for two ESPAR configurations including a 4-element linear dipole array and an 8-element rectangular PIFA array each with one feeding element. The frequency considered is 2.45 GHz where the wavelength λ is 122 mm. Perfect electric conductors (PEC) have been assumed in the simulations, however the effect of using low loss conductors is minimal. Full electromagnetic simulation (using CST studio suite) is used to obtain the open circuit radiation patterns $\mathbf{e}_i^{\text{oc}}(\Omega)$ for each element. However this only needs to be performed once for each element, since all other patterns can be formed from these using (4) [49]. This reduces the computation complexity of the simulation enormously as full electromagnetic simulation is not needed during the optimization, capacity or error performance simulation stages. In all the results provided we also include the post-optimization practical component constraints highlighted in the final paragraph of the previous section.

The structure of the 4-element linear dipole array is shown in Fig. 7. In this example the dipoles have length $l = 47$ mm and radius 2 mm and are placed along the x-axis with separation distance $R = 0.1\lambda$. The eigenvectors are listed in Table I and follow the form derived in (24). From (31) we obtain the initial point $\mathbf{X}_{n,\text{init}}^L$ as input for each mode in our algorithm. The optimal loads at 2.45 GHz for each mode are also listed in Table I through optimization and their corresponding four radiation patterns are shown in Fig. 8. While the feed port also requires a reactive load it should be noted that additional dynamic matching [34], [36], [37] can

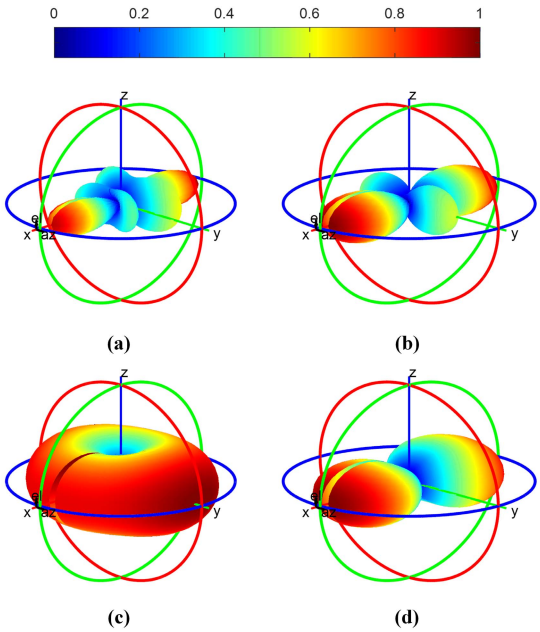

Fig. 8. Simulated antenna patterns for each orthogonal mode of the 4-element linear dipole array.

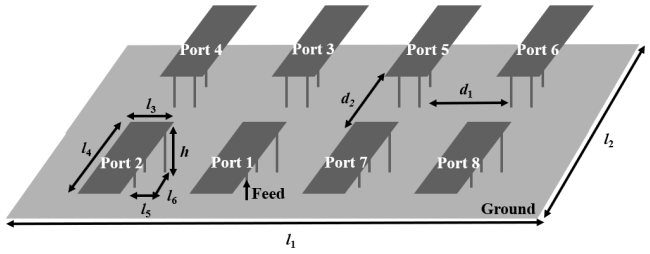

Fig. 9. 8-element rectangular PIFA Array.

be straightforwardly employed to maintain 50 Ω impedance matching for this port.

The structure of the 8-element rectangular PIFA array is shown in Fig. 9. Eight PIFA elements are placed in a 2×4 array. The length and width of the ground plane is $l_1 = 48$ mm and $l_2 = 90$ mm, respectively. The distances between two adjacent PIFAs are $d_1 = 0.1\lambda$ and $d_2 = 0.15\lambda$ as shown in Fig. 9. Other parameters are as follows: $l_3 = 5$ mm, $l_4 = 26$ mm, $l_5 = 2.4$ mm, $l_6 = 5$ mm and $h = 7$ mm. The eigenvectors for this configuration are listed in Table II and follow the form derived in (12). The optimal load combinations are also listed in Table II. Exciting Port 1, the radiation patterns obtained are as shown in Fig. 10.

The channel model utilized in the simulations is based on the beamspace domain interpretation of the conventional MIMO signal model [3]. Assuming a frequency-flat channel model, the system model of conventional MIMO with N transmit antennas and M receive antennas is

$$\mathbf{y} = \mathbf{H}\mathbf{x} + \mathbf{n} \tag{33}$$

where $\mathbf{H} \in \mathbb{C}^{M\times N}$ is the complex channel matrix, $\mathbf{n} \in \mathbb{C}^{M\times 1}$ is the additive Gaussian noise vector, $\mathbf{x} \in \mathbb{C}^{N\times 1}$ is the transmit signal, and $\mathbf{y} \in \mathbb{C}^{M\times 1}$ is the received signal. When using

TABLE II

EIGENVECTORS AND LOADS OF 8-ELEMENT RECTANGULAR PIFA ARRAY AT 2.45GHZ

Eigenvectors	Mode 1	Mode 2	Mode 3	Mode 4
Port 1	0.48	-0.48	0.34	0.36
Port 2	-0.14	0.14	-0.36	-0.34
Port 3	-0.48	-0.48	-0.34	0.36
Port 4	0.14	0.14	0.36	-0.34
Port 5	0.48	0.48	-0.34	0.36
Port 6	-0.14	-0.14	0.36	-0.34
Port 7	-0.48	0.48	0.34	0.36
Port 8	0.14	-0.14	-0.36	-0.34
Eigenvectors	Mode 5	Mode 6	Mode 7	Mode 8
Port 1	-0.36	-0.13	0.38	-0.19
Port 2	-0.34	-0.48	0.31	-0.46
Port 3	0.36	0.13	0.38	-0.19
Port 4	0.34	0.48	0.31	-0.46
Port 5	0.36	-0.13	0.38	0.19
Port 6	0.34	-0.48	0.31	0.46
Port 7	-0.36	0.13	0.38	0.19
Port 8	-0.34	0.48	0.31	0.46
Loads	Mode 1	Mode 2	Mode 3	Mode 4
Port 1	2.4 nH	2.1 nH	2.0 nH	1.1 nH
Port 2	2.2 nH	3.0 nH	2.1 nH	1.9 nH
Port 3	2.4 nH	2.1 nH	2.2 nH	1.5 nH
Port 4	1.9 nH	3.1 nH	2.1 nH	1.7 nH
Port 5	2.4 nH	2.1 nH	1.5 nH	0.1 nH
Port 6	1.9 nH	3.1 nH	2.2 nH	0.5 nH
Port 7	2.3 nH	2.1 nH	0.1 nH	1.0 nH
Port 8	2.3 nH	3.1 nH	2.0 nH	1.4 nH
Loads	Mode 5	Mode 6	Mode 7	Mode 8
Port 1	2.7 nH	0.8 pF	0.3 pF	6.8 pF
Port 2	2.9 nH	1.0 pF	1.6 nH	1.4 nH
Port 3	2.1 nH	2.2 nH	1.3 nH	2.0 nH
Port 4	2.5 nH	1.5 nH	4.0 nH	0.5 pF
Port 5	4.2 nH	2.7 nH	1.8 pF	2.3 nH
Port 6	6.0 nH	13.0 nH	13.0 nH	1.3 pF
Port 7	2.9 nH	2.1 nH	1.9 nH	2.3 nH
Port 8	11.5 nH	3.9 nH	5.1 nH	1.5 nH

ESPAR at the transmitter for single-RF MIMO we use transmit signals that are orthogonal or near orthogonal patterns rather than by utilizing different antenna elements. The formulation in (33) is modified using a virtual channel representation [29], [50] in the beamspace domain. Using the approach adopted in [50] the three-dimensional (3D) system model is written as

$$\begin{aligned}\mathbf{y} &= \mathbf{H}\mathbf{x} + \mathbf{n} = \mathbf{A}_R^H \mathbf{H}_v \mathbf{A}_T \mathbf{x} + \mathbf{n} \\ &= \mathbf{A}_R^H \mathbf{H}_v \mathbf{B}_T \mathbf{x}_{\text{bs}} + \mathbf{n} = \mathbf{H}_{\text{bs}} \mathbf{x}_{\text{bs}} + \mathbf{n},\end{aligned} \tag{34}$$

where $\mathbf{H}_v \in \mathbb{C}^{K\times K}$ is the virtual channel matrix representing the angular response of the discrete scatters and will depend on the underlying beamspace channel model [31]. For small angular resolution $\Delta\Omega$, entries in $\mathbf{H}_v$ refer to the channel gain from each angle of departure (AoD) to each angle of arrival (AoA) [50]. The steering matrices $\mathbf{A}_R = [\mathbf{a}_{R,1}, \mathbf{a}_{R,2}, \ldots, \mathbf{a}_{R,M}] \in \mathbb{C}^{K\times M}$ and $\mathbf{A}_T = [\mathbf{a}_{T,1}, \mathbf{a}_{T,2}, \ldots, \mathbf{a}_{T,N}] \in \mathbb{C}^{K\times N}$ in which $\mathbf{a}_{R,m} \in \mathbb{C}^{K\times 1}$ and $\mathbf{a}_{T,n} \in \mathbb{C}^{K\times 1}$ sample the patterns of the M receive and N transmit antennas respectively at K virtual channel angles in the beamspace domain. Using the N-element ESPAR as the transmit antenna in the beamspace formulation of MIMO, we have $\mathbf{A}_T\mathbf{x} = \mathbf{B}_T\mathbf{x}_{\text{bs}}$ where $\mathbf{B}_T = [\mathbf{b}_{T,1}, \mathbf{b}_{T,2}, \ldots, \mathbf{b}_{T,N_{\text{eff}}}] \in \mathbb{C}^{K\times N_{\text{eff}}}$ is the matrix

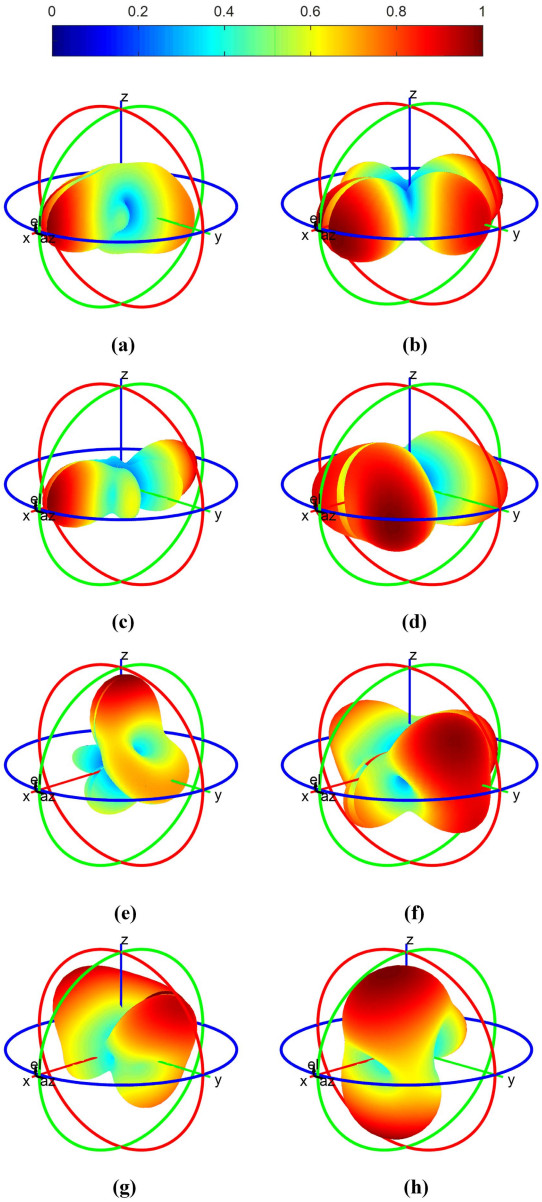

Fig. 10. Simulated antenna patterns for each orthogonal mode of the 8-element rectangular PIFA array.

consisting of N_{eff} orthogonal basis patterns, $\mathbf{x} \in \mathbb{C}^{N\times 1}$ and $\mathbf{x}_{\text{bs}} \in \mathbb{C}^{N_{\text{eff}}\times 1}$ are symbols in the conventional MIMO and beamspace domain respectively and N_{eff} is EADoF of the ESPAR [8], [33]. Then $\mathbf{H}_{\text{bs}} = \mathbf{A}_R^H \mathbf{H}_v \mathbf{B}_T$ is the beamspace channel matrix consisting of channel gains between steering matrices of the orthogonal transmit patterns and the conventional spatially separated receive antennas. We can therefore think of each element in $\mathbf{x}_{\text{bs}}$ as the transmission of an orthogonal pattern in the beamspace domain instead of the transmission on a separate antenna as we do for $\mathbf{x}$. Detection of the transmit signal $\mathbf{x}_{\text{bs}}$ at the receiver using a maximum-likelihood (ML) detector can then be written as

$$\tilde{\mathbf{x}}_{\text{bs}} = \underset{\mathbf{x}_{\text{bs}}}{\text{argmin}} ||\mathbf{y} - \mathbf{H}_{\text{bs}}\mathbf{x}_{\text{bs}}||. \tag{35}$$

In the numerical simulations provided in this work the angular resolution considered is $\Delta\phi = 5°$ and $\Delta\theta = 5°$ so that $K = 2664$ sampling points across the uniformly sampled 3D spherical space are utilized. Additive Gaussian noise $\mathbf{n}$ follows $\mathcal{CN}(0, N_0\mathbf{U}_N)$ with noise power N_0 and the signal-to-noise (SNR) is $\text{SNR} = P/N_0 = \|\mathbf{x}_{\text{bs}}\|^2/N_0 = 1/N_0$ where the average transmitted power P of the symbol $\mathbf{x}_{\text{bs}}$ is taken as unity. Assuming a rich scattering environment, entries in $\mathbf{H}_v$ satisfy $[\mathbf{H}_v]_{ij} \sim \mathcal{CN}(0,1)$ for $i,j = 1,2,\ldots,K$. Results follow for applying the two ESPAR configurations described above for SM-MISO and full multiplexed MIMO.

A. SM-MISO

We provide SE, EE and SER results for SM-MISO system in order to demonstrate the effectiveness of using TCM to obtain orthogonal patterns. The ESPAR's consisting of the 4-element linear dipole array and 8-element rectangular PIFA array described previously are used at the transmitter. At the receiver the single receive antenna is taken to be isotropic so that $\mathbf{A}_R = \mathbf{a}_{R,1}$ and $[\mathbf{a}_{R,1}]_k = \frac{1}{\sqrt{K}}$, $k = 1,2,\ldots,K$. At the transmitter $\mathbf{b}_{T,n}$ refers to each of the $N_{\text{eff}} = N = 4$ or 8 orthogonal ESPAR patterns which is used to transmit one symbol in turn in SM so that only one element of $\mathbf{x}_{\text{bs}}$ is unity and the others are all set to zero.

SM capacity or SE [4] can be written as

$$C_{\text{SM}} = \frac{1}{N_{\text{eff}}} \sum_{i=1}^{N_{\text{eff}}} \Bigg(\log_2 \left(\det \left(\mathbf{U}_M + \text{SNR}\, \|\mathbf{h}_i\|^2 \right) \right) + \int_y p(y \mid \mathbf{h}_i) \log_2 \frac{p(y \mid \mathbf{h}_i)}{p(y)} \text{d}y \Bigg), \tag{36}$$

where $\mathbf{H}_{\text{bs}} = [\mathbf{h}_1, \mathbf{h}_2, \ldots, \mathbf{h}_N]$, $\mathbf{h}_i \in \mathbb{C}^{M\times 1}$, $p(y \mid \mathbf{h}_i) = \frac{1}{\pi\left(P\|\mathbf{h}_i\|^2 + N_0\right)} \exp\left(\frac{|y|^2}{P\|\mathbf{h}_i\|^2 + N_0} \right)$, $p(y) = \frac{1}{N_{\text{eff}}} \sum_{i=1}^{N_{\text{eff}}} p(y \mid \mathbf{h}_i)$. Following the previous approach in [20], we define EE as

$$\text{EE} = \frac{C}{N_{\text{RF}} P_{\text{AC}} + P_0 + P_{\text{PA}}}, \tag{37}$$

where C is the capacity, N_{RF} is 1 for ESPAR and SM-MISO while N_{RF} is 4 or 8 for conventional MISO, P_{AC} is the constant RF circuit power consumption per antenna which is assumed as 33 dBm, P_0 is the power consumption for baseband processing assumed as 40 dBm. P_{PA} is the power consumption for power amplifier $P_{\text{PA}} = (1/\varepsilon - 1)P/e_{\text{ant}}$ where $\varepsilon = 0.35$ is efficiency of amplifier, P is the total transmit power, $e_{\text{ant}} = e_{\text{S}_{11}} e_{\text{rad}}$ is total efficiency of antenna. Assuming the antenna material is PEC and the loads are pure reactance we can assume that there is no power loss in the antenna so that $e_{\text{rad}} = 1$. Assuming the antenna is matched to have -10dB reflection coefficient that $e_{\text{S}_{11}} = 0.9$.

The simulated SE and EE of SM-MISO using ESPAR is shown in Fig. 11. In the results, ESPAR-SM-MISO is used to denote the ESPAR implementation of the system using either our 4-element linear dipole array or 8-element rectangular PIFA array. In addition the terms, ideal TCM patterns, and actual patterns refer to orthogonal patterns calculated from TCM and the actual patterns using optimization with practical component constraints as described in Section IV respectively. SM-MISO, MISO and SISO are used to indicate conventional spatial implementations of these systems where the antennas

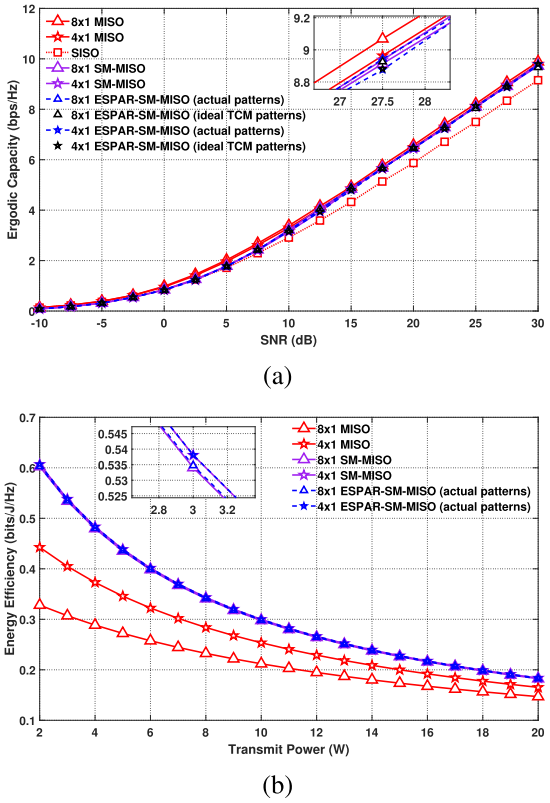

Fig. 11. Simulated performance of the ESPAR system in SM-MISO systems. (a) SE and (b) EE at SNR $= 30$ dB.

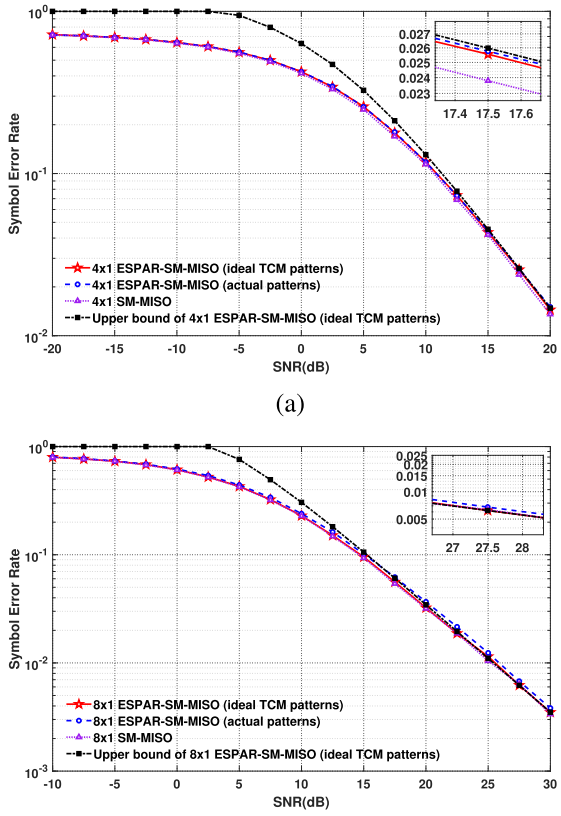

Fig. 12. Simulated SER performance of the ESPAR system in SM-MISO systems. (a) 4-element linear dipole array and (b) 8-element rectangular PIFA array.

are spatially separated and mutual coupling and channel correlation is taken as negligible. It can be observed that using actual patterns found by our proposed method, the ESPAR antenna achieves almost the same SE as SM-MISO. It is slightly lower than MISO as found in previous work since (36) takes a different form from MISO capacity [4]. In terms of EE the same conclusions hold again as for SM-MISO when compared to ESPAR-SM-MISO.

We also obtain simulated SER performance as a further verification of performance for SM-MISO as shown in Fig. 12 for the 4 and 8 transmit antenna configurations. The transmitted signal utilizes uncoded on-off keying (OOK) modulation without equalization and perfect channel state information (CSI) is assumed at the receiver. The number of symbol transmissions used in the simulation is 10^7. From Fig. 12, it is observed again that there is very little gap between the ideal and actual patterns as well as SM-MISO with spatially separated antennas. This shows again that our proposed algorithm has good performance in finding the load reactance to excite the desired modal radiation patterns from TCM. For reference the union bound of orthogonal modulation has almost the same SER as the TCM orthogonal patterns when SNR is high.

The advantage of using ESPAR in this application is that it has much smaller antenna array size using our proposed ESPAR due to smaller separation between elements (for example 0.1λ for the linear array) than conventional spatially separated antennas which would need up to 0.5λ spacing for a uniform linear or rectangular array.

B. Full Multiplexed MIMO

We also investigate the performance of ESPAR transmission for MIMO transmission configured to achieve full multiplexing following previous configurations [15], [31]. The transmitter is again configured as an ESPAR in which the transmitted symbols are $\mathbf{x}_{\text{bs}} = [x_{\text{bs},1}, x_{\text{bs},2}, \ldots, x_{\text{bs},N}]^T$ where the individual entries can be arbitrarily selected to form any constellation for MIMO transmission but must satisfy $||\mathbf{x}_{\text{bs}}|| = 1$. The radiation pattern $\mathbf{e}^r(\Omega) = \sum_{n=1}^{N} x_{\text{bs},n}\mathbf{e}_n(\Omega)$ is a linear combination of modal radiation patterns. The reactance loads for this configuration need to be switched for each constellation point, which can be found by referring to Section IV. B. The receiver is configured as a conventional uncoupled MIMO antenna with $\mathbf{A}_R\mathbf{A}_R^H = \mathbf{U}_M$.

Capacity or SE of full multiplexed MIMO can then be written as

$$C_{\text{BS}-\text{MIMO}} = \log_2\left(\det\left(\mathbf{U}_M + \frac{\text{SNR}}{N_{\text{eff}}}\mathbf{H}_{\text{bs}}\mathbf{H}_{\text{bs}}^H\right)\right). \quad (38)$$

By replacing N_{eff} with N and $\mathbf{H}_{\text{bs}}$ with $\mathbf{H}$, then (38) is also obtained for conventional spatially multiplexed MIMO. We also follow [20] to calculate EE similarly to (37). The simulated results for SE and EE are shown in Fig. 13 which also agree with previous work. In the simulations MIMO is utilized to denote a conventional MIMO system at both the receiver and transmitter with negligible mutual coupling

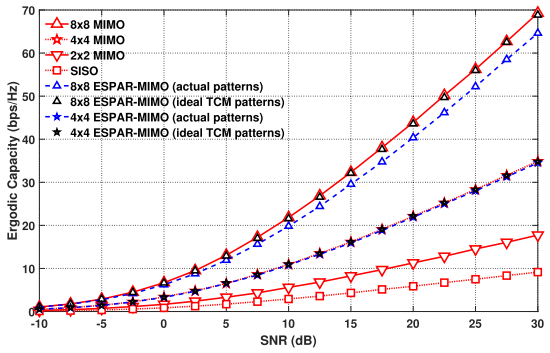

(a)

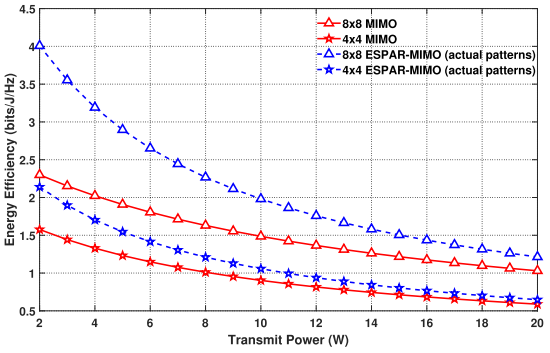

(b)

Fig. 13. Simulated performance of the ESPAR system in full multiplexed single-RF MIMO systems. (a) SE and (b) EE at SNR $= 30$ dB.

and channel correlation. It can be observed that using actual patterns (with practical component constraints) found by our proposed method, the ESPAR antenna achieves the same or nearly the same capacity as conventional MIMO. The small gap between 8×8 MIMO and ESPAR-MIMO (actual patterns) is caused by small correlations between actual patterns. EE of ESPAR is again significantly higher than conventional MIMO due to the reduced number of RF chains as expected.

VI. Conclusion

We have proposed a systematic method for finding orthogonal radiation patterns of ESPAR antennas based on N-port TCM. We also provide an efficient optimization method for finding the necessary load reactances to excite the desired orthogonal modal patterns. The resultant patterns can be used to form a pattern basis set for SM and full multiplexed MIMO. Simulation results of SE and EE for SM-MISO and full multiplexed MIMO for a 4-element linear array and an 8-element rectangular PIFA array are used to demonstrate the effectiveness of the approach.

Three limitations of the approach can be identified. The first is the PEC assumption in the antenna simulations. This can be overcome by extensions of N-port TCM to realistic materials [51]. However for low loss materials the effect is minimal.

The second limitation concerns the space over which the N-port TCM basis is found. In N-port TCM that space is the full spherical space of a sphere. In wireless communications the spherical space of interest is often more toroidal in shape so that radiation arriving in predominantly horizontal directions can be modeled. Therefore our results also need to be extended to subsets of the full spherical space. The fundamental point however is that over the full sphere only N TCM basis functions are required to represent all the possible radiation patterns. Therefore over subsets of this space the number of TCM basis functions required will be the same or less. Exploring the implications of this will be investigated in our future research.

The third limitation is the possible extension of the technique to massive MIMO. Due to the size of the massive MIMO array, mutual coupling between the driven element and some elements will be non-existent. Therefore ESPAR cannot be directly applied. To overcome this issue we could increase the number of driven elements by spacing them across the ESPAR so that every parasitic element would be in the presence of at least one driven element. Optimization for the loads as in Section IV. B to find patterns that are highly correlated with modal radiation patterns could be performed. While the disadvantage is that there would be multiple driven elements, in principle these could be obtained from a single-RF system using splitters or switches. This could also be an interesting idea to explore and to confirm whether the extension to massive ESPAR is indeed possible.

Appendix A
Derivation of Mode Matrix

The structure of the mode matrix, $\mathbf{M}$, for various array configurations is derived.

A. Rectangular Array

The structure of the resistance and reactance matrices for the 4-element rectangular array is

$$\mathbf{R},\mathbf{X} = \begin{bmatrix} a_{R,X} & b_{R,X} & c_{R,X} & d_{R,X} \\ b_{R,X} & a_{R,X} & d_{R,X} & c_{R,X} \\ c_{R,X} & d_{R,X} & a_{R,X} & b_{R,X} \\ d_{R,X} & c_{R,X} & b_{R,X} & a_{R,X} \end{bmatrix}, \tag{39}$$

where the subscripts refer to resistance and reactance respectively. The inverse of $\mathbf{R}$ is $\mathbf{R}^{-1} = \frac{\mathrm{adj}(\mathbf{R})}{\det(\mathbf{R})}$ where $\mathrm{adj}\,(\mathbf{R})$ is the adjugate matrix of $\mathbf{R}$. It is not difficult to verify that entries in $\mathrm{adj}\,(\mathbf{R})$ have the same structure as $\mathbf{R}$, so we denote $\mathbf{R}^{-1}$ and $\mathbf{M}$ as

$$\mathbf{R}^{-1} = \begin{bmatrix} a_{R^{-1}} & b_{R^{-1}} & c_{R^{-1}} & d_{R^{-1}} \\ b_{R^{-1}} & a_{R^{-1}} & d_{R^{-1}} & c_{R^{-1}} \\ c_{R^{-1}} & d_{R^{-1}} & a_{R^{-1}} & b_{R^{-1}} \\ d_{R^{-1}} & c_{R^{-1}} & b_{R^{-1}} & a_{R^{-1}} \end{bmatrix},$$

$$\mathbf{M} = \mathbf{R}^{-1}\mathbf{X} = \begin{bmatrix} a & b & c & d \\ b & a & d & c \\ c & d & a & b \\ d & c & b & a \end{bmatrix}. \tag{40}$$

For eigendecomposition we solve $\det(\lambda\mathbf{U}_4 - \mathbf{M}) = 0$ where the solution for the eigenvalues is $\lambda_1 = a+b+c+d$, $\lambda_2 = a-b-c+d$, $\lambda_3 = a-b+c-d$, $\lambda_4 = a+b-c-d$.

The corresponding eigenvectors with unity norm can then be obtained and are as shown in (11).

In the general case for a nested array, a, b, c, d in (10) become matrices $\mathbf{A}, \mathbf{B}, \mathbf{C}, \mathbf{D} \in \mathbb{R}^{pq\times pq}$ such that $\mathbf{M} \in \mathbb{R}^{4pq\times 4pq}$. We use the matrix similarity transformation to obtain the eigenvalues as well as the eigenvectors. Introducing the invertible matrix $\mathbf{P} \in \mathbb{R}^{4pq\times 4pq}$ as

$$\mathbf{P} = \frac{1}{2}\begin{bmatrix} \mathbf{U}_{pq} & \mathbf{U}_{pq} & \mathbf{U}_{pq} & \mathbf{U}_{pq} \\ \mathbf{U}_{pq} & -\mathbf{U}_{pq} & -\mathbf{U}_{pq} & \mathbf{U}_{pq} \\ \mathbf{U}_{pq} & -\mathbf{U}_{pq} & \mathbf{U}_{pq} & -\mathbf{U}_{pq} \\ \mathbf{U}_{pq} & \mathbf{U}_{pq} & -\mathbf{U}_{pq} & -\mathbf{U}_{pq} \end{bmatrix}, \tag{41}$$

where $\mathbf{P}^{-1} = \mathbf{P}$. From similarity transformation we obtain the similar matrix $\tilde{\mathbf{M}}$ given by $\tilde{\mathbf{M}} = \mathbf{P}^{-1}\mathbf{M}\mathbf{P} = \mathrm{diag}\big(\mathbf{A}+\mathbf{B}+\mathbf{C}+\mathbf{D}, \mathbf{A}-\mathbf{B}-\mathbf{C}+\mathbf{D}, \mathbf{A}-\mathbf{B}+\mathbf{C}-\mathbf{D}, \mathbf{A}+\mathbf{B}-\mathbf{C}-\mathbf{D}\big)$, so eigenvalues of $\mathbf{M}$ are eigenvalues of $\mathbf{A}+\mathbf{B}+\mathbf{C}+\mathbf{D}$, $\mathbf{A}-\mathbf{B}-\mathbf{C}+\mathbf{D}$, $\mathbf{A}-\mathbf{B}+\mathbf{C}-\mathbf{D}$ and $\mathbf{A}+\mathbf{B}-\mathbf{C}-\mathbf{D}$. For each diagonal block in $\tilde{\mathbf{M}}$, we have $(\mathbf{A}+\mathbf{B}+\mathbf{C}+\mathbf{D})\,\tilde{\mathbf{i}}_{1,n} = \lambda_{1,n}\tilde{\mathbf{i}}_{1,n}$, $(\mathbf{A}-\mathbf{B}-\mathbf{C}+\mathbf{D})\,\tilde{\mathbf{i}}_{2,n} = \lambda_{2,n}\tilde{\mathbf{i}}_{2,n}$, $(\mathbf{A}-\mathbf{B}+\mathbf{C}-\mathbf{D})\,\tilde{\mathbf{i}}_{3,n} = \lambda_{3,n}\tilde{\mathbf{i}}_{3,n}$, $(\mathbf{A}+\mathbf{B}-\mathbf{C}-\mathbf{D})\,\tilde{\mathbf{i}}_{4,n} = \lambda_{4,n}\tilde{\mathbf{i}}_{4,n}$ where $\tilde{\mathbf{i}}_{1,n}$, $\tilde{\mathbf{i}}_{2,n}$, $\tilde{\mathbf{i}}_{3,n}$, $\tilde{\mathbf{i}}_{4,n} \in \mathbb{R}^{pq\times 1}$ for $n = 1, 2, \ldots, pq$ are the eigenvectors of $\mathbf{A}+\mathbf{B}+\mathbf{C}+\mathbf{D}$, $\mathbf{A}-\mathbf{B}-\mathbf{C}+\mathbf{D}$, $\mathbf{A}-\mathbf{B}+\mathbf{C}-\mathbf{D}$ and $\mathbf{A}+\mathbf{B}-\mathbf{C}-\mathbf{D}$, respectively. Letting $\hat{\mathbf{I}}_m = \left[\tilde{\mathbf{i}}_{m,1}\ \tilde{\mathbf{i}}_{m,2}\ \ldots\ \tilde{\mathbf{i}}_{m,pq}\right] \in \mathbb{R}^{pq\times pq}$ for $m = 1, 2, 3, 4$, and block matrix $\mathbf{Q} = \mathrm{diag}\left(\hat{\mathbf{I}}_1, \hat{\mathbf{I}}_2, \hat{\mathbf{I}}_3, \hat{\mathbf{I}}_4\right)$ we obtain $\tilde{\mathbf{M}}\mathbf{Q} = \mathrm{diag}\left(\hat{\mathbf{I}}_1\mathbf{\Lambda}_1, \hat{\mathbf{I}}_2\mathbf{\Lambda}_2, \hat{\mathbf{I}}_3\mathbf{\Lambda}_3, \hat{\mathbf{I}}_4\mathbf{\Lambda}_4\right) = \mathbf{Q}\mathbf{\Lambda}$ where $\mathbf{\Lambda}_m = \mathrm{diag}(\lambda_{m,1}, \lambda_{m,2}, \ldots, \lambda_{m,pq})$ for $m = 1, 2, 3, 4$ and $\mathbf{\Lambda} = \mathrm{diag}\left(\mathbf{\Lambda}_1, \mathbf{\Lambda}_2, \mathbf{\Lambda}_3, \mathbf{\Lambda}_4\right)$. Therefore, we have $\mathbf{MPQ} = \mathbf{PQ\Lambda}$ so that $\mathbf{PQ}$ is the eigenmatrix given by

$$\mathbf{PQ} = \frac{1}{2}\begin{bmatrix} \hat{\mathbf{I}}_1 & \hat{\mathbf{I}}_2 & \hat{\mathbf{I}}_3 & \hat{\mathbf{I}}_4 \\ \hat{\mathbf{I}}_1 & -\hat{\mathbf{I}}_2 & -\hat{\mathbf{I}}_3 & \hat{\mathbf{I}}_4 \\ \hat{\mathbf{I}}_1 & -\hat{\mathbf{I}}_2 & \hat{\mathbf{I}}_3 & -\hat{\mathbf{I}}_4 \\ \hat{\mathbf{I}}_1 & \hat{\mathbf{I}}_2 & -\hat{\mathbf{I}}_3 & -\hat{\mathbf{I}}_4 \end{bmatrix}. \tag{42}$$

Each column of $\mathbf{PQ}$ is an eigenvector of $\mathbf{M}$, so that all the eigenvectors of $\mathbf{M}$ can be classified into the four forms as shown in (12).

B. Circular Array With Center Feeding

For the 5-element circular array with center feeding, $\mathbf{R}$ and $\mathbf{X}$ are written as

$$\mathbf{R}, \mathbf{X} = \begin{bmatrix} a_{R,X} & b_{R,X} & b_{R,X} & b_{R,X} & b_{R,X} \\ b_{R,X} & c_{R,X} & d_{R,X} & e_{R,X} & d_{R,X} \\ b_{R,X} & d_{R,X} & c_{R,X} & d_{R,X} & e_{R,X} \\ b_{R,X} & e_{R,X} & d_{R,X} & c_{R,X} & d_{R,X} \\ b_{R,X} & d_{R,X} & e_{R,X} & d_{R,X} & c_{R,X} \end{bmatrix}, \tag{43}$$

$\mathbf{R}^{-1}$ has same structure as $\mathbf{R}$, thus the mode matrix $\mathbf{M}$ has the form (13). Solution of the eigenvalues are $\lambda_{1,2} = \frac{a+d+2e+f\pm\sqrt{(d+2e+f-a)^2+16bc}}{2}$, $\lambda_3 = d-2e+f$, $\lambda_4 = \lambda_5 = d-f$. The corresponding eigenvectors with unity norm can then be found as in Section III. A. 2.

In the general N element case, the mode matrix $\mathbf{M}$ has the form (17). We firstly define an invertible matrix $\mathbf{P} \in \mathbb{R}^{N\times N}$ and matrix $\mathbf{M}_1 \in \mathbb{R}^{\frac{N+1}{2}\times\frac{N+1}{2}}$

$$\mathbf{P} = \begin{bmatrix} 1 & \mathbf{0}^T_{\frac{N-1}{2}} & \mathbf{0}^T_{\frac{N-1}{2}} \\ \mathbf{0}_{\frac{N-1}{2}} & \frac{1}{\sqrt{2}}\mathbf{U}_{\frac{N-1}{2}} & \frac{1}{\sqrt{2}}\mathbf{U}_{\frac{N-1}{2}} \\ \mathbf{0}_{\frac{N-1}{2}} & \frac{1}{\sqrt{2}}\mathbf{U}_{\frac{N-1}{2}} & -\frac{1}{\sqrt{2}}\mathbf{U}_{\frac{N-1}{2}} \end{bmatrix},$$
$$\mathbf{M}_1 = \begin{bmatrix} a & \sqrt{2}\mathbf{b} \\ \sqrt{2}\mathbf{c} & \mathbf{D}+\mathbf{E} \end{bmatrix}, \tag{44}$$

where $\mathbf{P}^{-1} = \mathbf{P}$. The similar matrix $\tilde{\mathbf{M}}$ is obtained from the similarity transformation $\tilde{\mathbf{M}} = \mathbf{P}^{-1}\mathbf{M}\mathbf{P} = \mathrm{diag}\,(\mathbf{M}_1, \mathbf{D}-\mathbf{E})$ so that eigenvalues of $\mathbf{M}$ are eigenvalues of $\mathbf{M}_1$ and $\mathbf{D}-\mathbf{E}$. Therefore we have $\mathbf{M}_1\bar{\mathbf{i}}_{1,n} = \lambda_{1,n}\bar{\mathbf{i}}_{1,n}$, $(\mathbf{D}-\mathbf{E})\,\bar{\mathbf{i}}_{2,n} = \lambda_{2,n}\bar{\mathbf{i}}_{2,n}$ where $\bar{\mathbf{i}}_{1,n} \in \mathbb{R}^{\frac{N+1}{2}\times 1}$, $n = 1, 2, \ldots, \frac{N+1}{2}$ and $\bar{\mathbf{i}}_{2,n} \in \mathbb{R}^{\frac{N-1}{2}\times 1}$, $n = 1, 2, \ldots, \frac{N-1}{2}$ are eigenvectors of $\mathbf{M}_1$ and $\mathbf{D}-\mathbf{E}$. Letting $\hat{\mathbf{I}}_1 = \left[\bar{\mathbf{i}}_{1,1}\ \bar{\mathbf{i}}_{1,2}\ \ldots\ \bar{\mathbf{i}}_{1,\frac{N+1}{2}}\right] \in \mathbb{R}^{\frac{N+1}{2}\times\frac{N+1}{2}}$, $\hat{\mathbf{I}}_2 = \left[\bar{\mathbf{i}}_{2,1}\ \bar{\mathbf{i}}_{2,2}\ \ldots\ \bar{\mathbf{i}}_{2,\frac{N-1}{2}}\right] \in \mathbb{R}^{\frac{N-1}{2}\times\frac{N-1}{2}}$ such that $\mathbf{Q} = \mathrm{diag}\left(\hat{\mathbf{I}}_1, \hat{\mathbf{I}}_2\right)$ we obtain $\tilde{\mathbf{M}}\mathbf{Q} = \mathrm{diag}\left(\hat{\mathbf{I}}_1\mathbf{\Lambda}_1, \hat{\mathbf{I}}_2\mathbf{\Lambda}_2\right) = \mathbf{Q\Lambda}$ where we define $\mathbf{\Lambda}_1 = \mathrm{diag}\left(\lambda_{1,1}, \lambda_{1,2}, \ldots, \lambda_{1,\frac{N+1}{2}}\right) \in \mathbb{R}^{\frac{N+1}{2}\times\frac{N+1}{2}}$, $\mathbf{\Lambda}_2 = \mathrm{diag}\left(\lambda_{2,1}, \lambda_{2,2}, \ldots, \lambda_{2,\frac{N-1}{2}}\right) \in \mathbb{R}^{\frac{N-1}{2}\times\frac{N-1}{2}}$, and $\mathbf{\Lambda} = \mathrm{diag}\,(\mathbf{\Lambda}_1, \mathbf{\Lambda}_2)$. So we have $\mathbf{MPQ} = \mathbf{PQ\Lambda}$ so that $\mathbf{PQ}$ is an eigenmatrix where each column is an eigenvector. By partitioning $\hat{\mathbf{I}}_1$ as $\left[\hat{\mathbf{I}}_1\right]_1 \in \mathbb{R}^{1\times\frac{N+1}{2}}$ which is the first row of $\hat{\mathbf{I}}_1$ and $\left[\hat{\mathbf{I}}_1\right]_{2,3,\ldots,\frac{N-1}{2}} \in \mathbb{R}^{\frac{N-1}{2}\times\frac{N+1}{2}}$ which is the remaining rows of $\hat{\mathbf{I}}_1$, we can rewrite $\mathbf{PQ}$ as

$$\mathbf{PQ} = \begin{bmatrix} \left[\hat{\mathbf{I}}_1\right]_1 & \mathbf{0}^T_{\frac{N-1}{2}} \\ \frac{1}{\sqrt{2}}\left[\hat{\mathbf{I}}_1\right]_{2,3,\ldots,\frac{N-1}{2}} & \frac{1}{\sqrt{2}}\hat{\mathbf{I}}_2 \\ \frac{1}{\sqrt{2}}\left[\hat{\mathbf{I}}_1\right]_{2,3,\ldots,\frac{N-1}{2}} & -\frac{1}{\sqrt{2}}\hat{\mathbf{I}}_2 \end{bmatrix}. \tag{45}$$

Therefore, the eigenvectors of $\mathbf{M}$ can be classified as the forms provided in (18).

C. Linear Array

Finally, in the 4-element linear array, $\mathbf{R}$ and $\mathbf{X}$ are written as

$$\mathbf{R}, \mathbf{X} = \begin{bmatrix} a_{R,X} & b_{R,X} & c_{R,X} & d_{R,X} \\ b_{R,X} & e_{R,X} & d_{R,X} & f_{R,X} \\ c_{R,X} & d_{R,X} & a_{R,X} & b_{R,X} \\ d_{R,X} & f_{R,X} & b_{R,X} & e_{R,X} \end{bmatrix}, \tag{46}$$

so that the mode matrix $\mathbf{M}$ has the form (19). Using $\det(\lambda\mathbf{U}_4 - \mathbf{M}) = 0$, the eigenvalues are $\lambda_{1,2} = \frac{(f+h+a+c)\pm\sqrt{(f+h-a-c)^2+4(b+d)(e+g)}}{2}$, $\lambda_{3,4} = \frac{(f-h+a-c)\pm\sqrt{(f-h-a+c)^2+4(b-d)(e-g)}}{2}$. The corresponding eigenvectors with unity norm can be obtained as shown in Section III. A. 3.

The mode matrix $\mathbf{M}$ for the generalized configuration in Section III. A. 3 is provided in (23). We can simplify $\mathbf{M}$ as

$$\mathbf{M} = \begin{bmatrix} \mathbf{M}_1 & \mathbf{M}_2 \\ \mathbf{M}_2 & \mathbf{M}_1 \end{bmatrix}, \mathbf{M}_1 = \begin{bmatrix} a & \mathbf{b} \\ \mathbf{e} & \mathbf{F} \end{bmatrix}, \mathbf{M}_2 = \begin{bmatrix} c & \mathbf{d} \\ \mathbf{g} & \mathbf{H} \end{bmatrix}, \quad (47)$$

where $\mathbf{M}_{1,2} \in \mathbb{R}^{\frac{N}{2} \times \frac{N}{2}}$. We define again an invertible matrix $\mathbf{P} \in \mathbb{R}^{N \times N}$ written as

$$\mathbf{P} = \frac{1}{\sqrt{2}} \begin{bmatrix} \mathbf{U}_{\frac{N}{2}} & \mathbf{U}_{\frac{N}{2}} \\ \mathbf{U}_{\frac{N}{2}} & -\mathbf{U}_{\frac{N}{2}} \end{bmatrix}, \quad (48)$$

where it can be shown straightforwardly that $\mathbf{P}^{-1} = \mathbf{P}$. The similar matrix $\tilde{\mathbf{M}}$ can be found as $\tilde{\mathbf{M}} = \mathbf{P}^{-1}\mathbf{M}\mathbf{P} = \operatorname{diag}(\mathbf{M}_1 + \mathbf{M}_2, \mathbf{M}_1 - \mathbf{M}_2)$. Therefore, eigenvalues of $\mathbf{M}$ are eigenvalues of $\mathbf{M}_1 + \mathbf{M}_2$ and $\mathbf{M}_1 - \mathbf{M}_2$. The following equations can then be obtained $(\mathbf{M}_1 + \mathbf{M}_2)\tilde{\mathbf{i}}_{1,n} = \lambda_{1,n}\tilde{\mathbf{i}}_{1,n}$, $(\mathbf{M}_1 - \mathbf{M}_2)\tilde{\mathbf{i}}_{2,n} = \lambda_{2,n}\tilde{\mathbf{i}}_{2,n}$ where $\tilde{\mathbf{i}}_{1,n}$ and $\tilde{\mathbf{i}}_{2,n} \in \mathbb{R}^{\frac{N}{2} \times 1}$ for $n = 1, 2, \ldots, \frac{N}{2}$ are eigenvectors of $\mathbf{M}_1 + \mathbf{M}_2$ and $\mathbf{M}_1 - \mathbf{M}_2$, respectively. Letting $\hat{\mathbf{I}}_1 = \left[\tilde{\mathbf{i}}_{1,1}\ \tilde{\mathbf{i}}_{1,2} \ldots \tilde{\mathbf{i}}_{1,\frac{N}{2}}\right] \in \mathbb{R}^{\frac{N}{2} \times \frac{N}{2}}$, $\hat{\mathbf{I}}_2 = \left[\tilde{\mathbf{i}}_{2,1}\ \tilde{\mathbf{i}}_{2,2} \ldots \tilde{\mathbf{i}}_{2,\frac{N}{2}}\right] \in \mathbb{R}^{\frac{N}{2} \times \frac{N}{2}}$, and $\mathbf{Q} = \operatorname{diag}\left(\hat{\mathbf{I}}_1, \hat{\mathbf{I}}_2\right)$ we obtain $\tilde{\mathbf{M}}\mathbf{Q} = \operatorname{diag}\left(\hat{\mathbf{I}}_1\mathbf{\Lambda}_1, \hat{\mathbf{I}}_2\mathbf{\Lambda}_2\right) = \mathbf{Q}\mathbf{\Lambda}$ where we define that $\mathbf{\Lambda}_1 = \operatorname{diag}\left(\lambda_{1,1}, \lambda_{1,2}, \ldots, \lambda_{1,\frac{N}{2}}\right)$, $\mathbf{\Lambda}_2 = \operatorname{diag}\left(\lambda_{2,1}, \lambda_{2,2}, \ldots, \lambda_{2,\frac{N}{2}}\right) \in \mathbb{R}^{\frac{N}{2} \times \frac{N}{2}}$, and $\mathbf{\Lambda} = \operatorname{diag}(\mathbf{\Lambda}_1, \mathbf{\Lambda}_2)$. So we have $\mathbf{M}\mathbf{P}\mathbf{Q} = \mathbf{P}\mathbf{Q}\mathbf{\Lambda}$ such that $\mathbf{P}\mathbf{Q}$ is an eigenmatrix where each column is an eigenvector and it is given by

$$\mathbf{P}\mathbf{Q} = \frac{1}{\sqrt{2}} \begin{bmatrix} \hat{\mathbf{I}}_1 & \hat{\mathbf{I}}_2 \\ \hat{\mathbf{I}}_1 & -\hat{\mathbf{I}}_2 \end{bmatrix}. \quad (49)$$

Therefore, the eigenvectors of $\mathbf{M}$ can be classified into the forms provided in (24).

REFERENCES

[1] E. Telatar, "Capacity of multi-antenna Gaussian channels," *Eur. Trans. Telecommun.*, vol. 10, no. 6, pp. 585–595, Nov. 1999.

[2] R. D. Murch and K. B. Letaief, "Antenna systems for broadband wireless access," *IEEE Commun. Mag.*, vol. 40, no. 4, pp. 76–83, Apr. 2002.

[3] M. Di Renzo, H. Haas, A. Ghrayeb, S. Sugiura, and L. Hanzo, "Spatial modulation for generalized MIMO: Challenges, opportunities, and implementation," *Proc. IEEE*, vol. 102, no. 1, pp. 56–103, Jan. 2014.

[4] A. Stavridis, S. Sinanovic, M. Di Renzo, and H. Haas, "Energy evaluation of spatial modulation at a multi-antenna base station," in *Proc. IEEE 78th Veh. Technol. Conf. (VTC Fall)*, Sep. 2013, pp. 1–5.

[5] O. E. Ayach, S. Rajagopal, S. Abu-Surra, Z. Pi, and R. W. Heath, Jr., "Spatially sparse precoding in millimeter wave MIMO systems," *IEEE Trans. Wireless Commun.*, vol. 13, no. 3, pp. 1499–1513, Mar. 2014.

[6] S. Han, C.-L. I, Z. Xu, and C. Rowell, "Large-scale antenna systems with hybrid analog and digital beamforming for millimeter wave 5G," *IEEE Commun. Mag.*, vol. 53, no. 1, pp. 186–194, Jan. 2015.

[7] Y. Li *et al.*, "Analog precoding using highly reconfigurable antennas," *IEEE Wireless Commun. Lett.*, vol. 9, no. 5, pp. 648–652, May 2020.

[8] A. Kalis, A. Kanatas, and C. Papadias, "A novel approach to MIMO transmission using a single RF front end," *IEEE J. Sel. Areas Commun.*, vol. 26, no. 6, pp. 972–980, Aug. 2008.

[9] A. Mohammadi and F. M. Ghannouchi, "Single RF front-end MIMO transceivers," in *RF Transceiver Design for MIMO Wireless Communication*. Berlin, Germany: Springer, 2012, pp. 265–288.

[10] R. Y. Mesleh, H. Haas, S. Sinanovic, C. W. Ahn, and S. Yun, "Spatial modulation," *IEEE Trans. Veh. Technol.*, vol. 57, no. 4, pp. 2228–2241, Jul. 2008.

[11] J. Jeganathan, A. Ghrayeb, and L. Szczecinski, "Spatial modulation: Optimal detection and performance analysis," *IEEE Commun. Lett.*, vol. 12, no. 8, pp. 545–547, Aug. 2008.

[12] T. Ohira and K. Gyoda, "Electronically steerable passive array radiator antennas for low-cost analog adaptive beamforming," in *Proc. IEEE Int. Conf. Phased Array Syst. Technol.*, May 2000, pp. 101–104.

[13] R. Ramirez-Gutierrez, L. Zhang, J. Elmirghani, and A. F. Almutairi, "Antenna beam pattern modulation for MIMO channels," in *Proc. 8th Int. Wireless Commun. Mobile Comput. Conf. (IWCMC)*, Aug. 2012, pp. 591–595.

[14] H. Kawakami and T. Ohira, "Electrically steerable passive array radiator (ESPAR) antennas," *IEEE Antennas Propag. Mag.*, vol. 47, no. 2, pp. 43–50, Apr. 2005.

[15] O. Alrabadi, C. Papadias, A. Kalis, and R. Prasad, "A universal encoding scheme for MIMO transmission using a single active element for PSK modulation schemes," *IEEE Trans. Wireless Commun.*, vol. 8, no. 10, pp. 5133–5142, Oct. 2009.

[16] J. Lee, Y. Lee, K. Lee, and T. Joong Kim, "λ/64-spaced compact ESPAR antenna via analog RF switches for a single RF chain MIMO system," *ETRI J.*, vol. 41, no. 4, pp. 536–548, Aug. 2019.

[17] K. Kumar Kishor and S. V. Hum, "A pattern reconfigurable chassis-mode MIMO antenna," *IEEE Trans. Antennas Propag.*, vol. 62, no. 6, pp. 3290–3298, Jun. 2014.

[18] B. Han, V. I. Barousis, C. B. Papadias, A. Kalis, and R. Prasad, "MIMO over ESPAR with 16-QAM modulation," *IEEE Wireless Commun. Lett.*, vol. 2, no. 6, pp. 687–690, Dec. 2013.

[19] D. J. Reinoso Chisaguano, Y. Hou, T. Higashino, and M. Okada, "Low-complexity channel estimation and detection for MIMO-OFDM receiver with ESPAR antenna," *IEEE Trans. Veh. Technol.*, vol. 65, no. 10, pp. 8297–8308, Oct. 2016.

[20] A. Li, C. Masouros, and C. B. Papadias, "MIMO transmission for single-fed ESPAR with quantized loads," *IEEE Trans. Commun.*, vol. 65, no. 7, pp. 2863–2876, Jul. 2017.

[21] A. Li, C. Masouros, and M. Sellathurai, "Analog–digital beamforming in the MU-MISO downlink by use of tunable antenna loads," *IEEE Trans. Veh. Technol.*, vol. 67, no. 4, pp. 3114–3129, Apr. 2018.

[22] A. Li and C. Masouros, "Exploiting constructive mutual coupling in P2P MIMO by analog-digital phase alignment," *IEEE Trans. Wireless Commun.*, vol. 16, no. 3, pp. 1948–1962, Mar. 2017.

[23] J. Lee, J. Y. Lee, and Y. H. Lee, "Spatial multiplexing of OFDM signals with QPSK modulation over ESPAR," *IEEE Trans. Veh. Technol.*, vol. 66, no. 6, pp. 4914–4923, Jun. 2017.

[24] D. Falconer, S. L. Ariyavisitakul, A. Benyamin-Seeyar, and B. Eidson, "Frequency domain equalization for single-carrier broadband wireless systems," *IEEE Commun. Mag.*, vol. 40, no. 4, pp. 58–66, Apr. 2002.

[25] H. Myung, J. Lim, and D. Goodman, "Single carrier FDMA for uplink wireless transmission," *IEEE Veh. Technol. Mag.*, vol. 1, no. 3, pp. 30–38, Sep. 2006.

[26] O. N. Alrabadi, J. Perruisseau-Carrier, and A. Kalis, "MIMO transmission using a single RF source: Theory and antenna design," *IEEE Trans. Antennas Propag.*, vol. 60, no. 2, pp. 654–664, Feb. 2012.

[27] M. Yousefbeiki and J. Perruisseau-Carrier, "Towards compact and frequency-tunable antenna solutions for MIMO transmission with a single RF chain," *IEEE Trans. Antennas Propag.*, vol. 62, no. 3, pp. 1065–1073, Mar. 2014.

[28] S. Zhang, I. Syrytsin, and G. F. Pedersen, "Compact beam-steerable antenna array with two passive parasitic elements for 5G mobile terminals at 28 GHz," *IEEE Trans. Antennas Propag.*, vol. 66, no. 10, pp. 5193–5203, Oct. 2018.

[29] A. M. Sayeed, "Deconstructing multiantenna fading channels," *IEEE Trans. Signal Process.*, vol. 50, no. 10, pp. 2563–2579, Oct. 2002.

[30] J. Brady, N. Behdad, and A. M. Sayeed, "Beamspace MIMO for millimeter-wave communications: System architecture, modeling, analysis, and measurements," *IEEE Trans. Antennas Propag.*, vol. 61, no. 7, pp. 3814–3827, Jul. 2013.

[31] V. I. Barousis, A. G. Kanatas, and A. Kalis, "Beamspace-domain analysis of single-RF front-end MIMO systems," *IEEE Trans. Veh. Technol.*, vol. 60, no. 3, pp. 1195–1199, Mar. 2011.

[32] V. Barousis and A. G. Kanatas, "Aerial degrees of freedom of parasitic arrays for single RF front-end MIMO transceivers," *Prog. Electromagn. Res. B*, vol. 35, pp. 287–306, 2011.

[33] P. N. Vasileiou, K. Maliatsos, E. D. Thomatos, and A. G. Kanatas, "Reconfigurable orthonormal basis patterns using ESPAR antennas," *IEEE Antennas Wireless Propag. Lett.*, vol. 12, pp. 448–451, 2013.

[34] M. A. Sedaghat, V. I. Barousis, R. R. Müller, and C. B. Papadias, "Load modulated arrays: A low-complexity antenna," *IEEE Commun. Mag.*, vol. 54, no. 3, pp. 46–52, Mar. 2016.

[35] M. A. Sedaghat, R. R. Mueller, G. Fischer, and A. Ali, "Discrete load-modulated single-RF MIMO transmitters," in *Proc. 20th Int. ITG Workshop Smart Antennas*. Frankfurt, Germany: VDE, 2016, pp. 1–7.

[36] H. T. Jeong, J. E. Kim, I. S. Chang, and C. D. Kim, "Tunable impedance transformer using a transmission line with variable characteristic impedance," *IEEE Trans. Microw. Theory Techn.*, vol. 53, no. 8, pp. 2587–2593, Aug. 2005.
[37] C. Sánchez-Pérez, J. de Mingo, P. L. Carro, and P. García-Dúcar, "Design and applications of a 300–800 MHz tunable matching network," *IEEE J. Emerg. Sel. Topics Circuits Syst.*, vol. 3, no. 4, pp. 531–540, Dec. 2013.
[38] V. I. Barousis, C. B. Papadias, and R. R. Muller, "A new signal model for MIMO communication with compact parasitic arrays," in *Proc. 6th Int. Symp. Commun., Control Signal Process. (ISCCSP)*, May 2014, pp. 109–113.
[39] R. J. Garbacz, "Modal expansions for resonance scattering phenomena," *Proc. IEEE*, vol. 53, no. 8, pp. 856–864, Aug. 1965.
[40] R. Garbacz and R. Turpin, "A generalized expansion for radiated and scattered fields," *IEEE Trans. Antennas Propag.*, vol. AP-19, no. 3, pp. 348–358, May 1971.
[41] R. Harrington and J. Mautz, "Theory of characteristic modes for conducting bodies," *IEEE Trans. Antennas Propag.*, vol. AP-19, no. 5, pp. 622–628, Sep. 1971.
[42] J. Mautz and R. Harrington, "Modal analysis of loaded N-port scatterers," *IEEE Trans. Antennas Propag.*, vol. AP-21, no. 2, pp. 188–199, Mar. 1973.
[43] Y. Chen and C.-F. Wang, "Synthesis of reactively controlled antenna arrays using characteristic modes and DE algorithm," *IEEE Antennas Wireless Propag. Lett.*, vol. 11, pp. 385–388, 2012.
[44] Y. Chen and C.-F. Wang, *Characteristic Modes: Theory and Applications in Antenna Engineering*. Hoboken, NJ, USA: Wiley, 2015.
[45] F. Jiang, C.-Y. Chiu, S. Shen, Q. S. Cheng, and R. Murch, "Pixel antenna optimization using N-Port characteristic mode analysis," *IEEE Trans. Antennas Propag.*, vol. 68, no. 5, pp. 3336–3347, May 2020.
[46] C. Y. Chiu, S. Shen, B. K. Lau, and R. Murch, "The design of a trimodal broadside antenna element for compact massive MIMO arrays: Utilizing the theory of characteristic modes," *IEEE Antennas Propag. Mag.*, early access, Dec. 31, 2019, doi: 10.1109/MAP.2019.2958515.
[47] C. D. Meyer, *Matrix Analysis and Applied Linear Algebra*, vol. 71. Philadelphia, PA, USA: SIAM, 2000.
[48] P. E. Gill and W. Murray, "Quasi-Newton methods for unconstrained optimization," *IMA J. Appl. Math.*, vol. 9, no. 1, pp. 91–108, Feb. 1972.
[49] P. Lotfi, S. Soltani, and R. D. Murch, "Printed endfire beam-steerable pixel antenna," *IEEE Trans. Antennas Propag.*, vol. 65, no. 8, pp. 3913–3923, Aug. 2017.
[50] K. Maliatsos and A. G. Kanatas, "Modifications of the IST-WINNER channel model for beamspace processing and parasitic arrays," in *Proc. 7th Eur. Conf. Antennas Propag.*, 2013, pp. 989–993.
[51] Z. T. Miers and B. K. Lau, "Computational analysis and verifications of characteristic modes in real materials," *IEEE Trans. Antennas Propag.*, vol. 64, no. 7, pp. 2595–2607, Jul. 2016.

Zixiang Han (Graduate Student Member, IEEE) received the bachelor's degree in electronic science and technology from the Nanjing University, Nanjing, China, in 2018. He is currently pursuing the Ph.D. degree with the Department of Electronic and Computer Engineering from The Hong Kong University of Science and Technology, Hong Kong. His current research interests include the theory of characteristic mode, MIMO systems, and MIMO antenna design.

Yujie Zhang (Graduate Student Member, IEEE) received the bachelor's degree in optoelectronic information science and engineering from the Huazhong University of Science and Technology, Wuhan, China, in 2017. He is currently pursuing the Ph.D. degree with the Department of Electronic and Computer Engineering, The Hong Kong University of Science and Technology, Hong Kong. His current research interests include the antenna design on the Internet-of-Things applications, RF energy harvesting, wireless power transmission, MIMO antenna design, and 5G.

Shanpu Shen (Member, IEEE) received the bachelor's degree in communication engineering from the Nanjing University of Science and Technology, Nanjing, China, in 2013, and the Ph.D. degree in electronic and computer engineering from The Hong Kong University of Science and Technology (HKUST), Hong Kong, in 2017.

He was a Visiting Ph.D. Student with the Microsystems Technology Laboratories, Massachusetts Institute of Technology, Cambridge, MA, USA, in 2016. He was a Post-Doctoral Fellow with HKUST from 2017 to 2018. He was a Post-Doctoral Research Associate with the Communications and Signal Processing Group, Imperial College London, London, U.K., from 2018 to 2020. He is currently a Research Assistant Professor with HKUST. His current research interests include RF energy harvesting, wireless power transfer, Internet-of-Things, MIMO systems, and antenna design and optimization.

Yue Li (Student Member, IEEE) received the B.S. degree in information science and electronic engineering from Zhejiang University, Hangzhou, China, in 2015, and the Ph.D. degree in electronic and computer engineering from The Hong Kong University of Science and Technology, Hong Kong, in 2019. His current research interests include smart water systems, Internet of Things, and wireless communication.

Chi-Yuk Chiu (Senior Member, IEEE) received the B.Eng. and M.Eng. degrees and the Ph.D. degree in electronic engineering from the City University of Hong Kong, in 2001, 2001, and 2005, respectively. He joined as a Research Assistant Professor the Department of Electronic and Computer Engineering (ECE), The Hong Kong University of Science and Technology (HKUST) in 2005. He was a Senior Antenna Engineer with Sony Mobile Communications, Beijing, in 2011. He joined as a Research Assistant Professor with the Department of ECE, HKUST, in 2015. He has authored or coauthored 84 articles and two book chapters. He holds several patents related to antenna technology. His main research interests include the design and analysis of small antennas, MIMO antennas, applications of characteristic modes, and energy harvesting. He is also a member of the IEEE Antennas and Propagation Society Education Committee.

Ross Murch (Fellow, IEEE) received the bachelor's and Ph.D. degrees in electrical and electronic engineering from the University of Canterbury, New Zealand.

He is currently the Chair Professor with the Department of Electronic and Computer Engineering, The Hong Kong University of Science and Technology (HKUST), where he is also a Senior Fellow with the Institute of Advanced Study. His research contributions include more than 300 publications, and 20 patents. He has successfully supervised 50 research graduate students. His current research interests include the Internet-of-Things, RF imaging, ambient RF systems, multiport antenna systems, and reconfigurable intelligent surfaces, with an emphasis on his combination of knowledge from both wireless communication systems and electromagnetic areas.

Dr. Murch was the Department Head with HKUST from 2009 to 2015. He is a fellow of IET and HKIE. He has served the IEEE in various positions, including the IEEE area editor, the technical program chair, a distinguished lecturer, and a fellow of the evaluation committee. He enjoys teaching and has received two teaching awards. He has received several awards, including the Computer Simulation Technology University Publication Award.